

Isolated flat bands in 2D lattices based on a path-exchange symmetry

Jun-Hyung Bae¹, Tigran Sedrakyan², Saurabh Maiti^{1,3}

¹ Department of Physics, Concordia University, Montreal, QC H4B 1R6, Canada

² Department of Physics, University of Massachusetts, Amherst, MA 01003, USA

³ Centre for Research in Molecular Modelling, Concordia University, Montreal, QC H4B 1R6, Canada

January 27, 2023

1 Abstract

2 The increased ability to engineer two-dimensional (2D) systems, either using
 3 materials, photonic lattices, or cold atoms, has led to the search for 2D struc-
 4 tures with interesting properties. One such property is the presence of flat
 5 bands. Typically, the presence of these requires long-ranged hoppings, fine-
 6 tuning of nearest neighbor hoppings, or breaking time-reversal symmetry by
 7 using a staggered flux distribution in the unit cell. We provide a prescription
 8 based on carrying out projections from a parent system to generate different
 9 flat band systems. We identify the conditions for maintaining the flatness and
 10 identify a path-exchange symmetry in such systems that cause the flat band to
 11 be degenerate with the other dispersive ones. Breaking this symmetry leads
 12 to lifting the degeneracy while still preserving the flatness of the band. This
 13 technique does not require changing the topology nor breaking time-reversal
 14 symmetry as was suggested earlier in the literature. The prescription also
 15 eliminates the need for any fine-tuning. Moreover, it is shown that the sub-
 16 sequent projected systems inherit the precise fine-tuning conditions that were
 17 discussed in the literature for similar systems, in order to have and isolate a
 18 flat band. As examples, we demonstrate the use of our prescription to arrive
 19 at the flat band conditions for popular systems like the Kagomé, the Lieb,
 20 and the Dice lattices. Finally, we are also able to show that a flat band ex-
 21 ists in a recently proposed chiral spin-liquid state of the Kagomé lattice only
 22 if it is associated with a gauge field that produces a flux modulation of the
 23 Chern-Simons type.

24

25 Contents

26	1 Introduction	2
27	2 Kagomé: naïve attempts to lift the flat band degeneracy	5
28	2.1 Onsite perturbations and strain	6
29	2.2 Breaking TRS	6
30	3 Kagomé: Flat band preserving parameterization	7
31	3.1 Physical meaning behind the r -parameter	9
32	3.2 Model with $ r > 1$	10

33	4 A prescription to generate flat band systems	11
34	4.1 Flat bands beyond the bipartite condition	14
35	5 Isolating the flat band	16
36	6 Application of the prescription to other lattices	18
37	6.1 Lieb lattice and its projections	19
38	6.2 Dice lattice and its projections	21
39	7 Flat band with Chern-Simons flux distribution	23
40	8 Conclusion	26
41	A Useful relations between matrix elements $\tilde{\alpha}_i$	27
42	B Properties of non-square matrices	28
43	C Identifying the path-exchange symmetry	28
44	References	29

1 Introduction

The term ‘flat band systems’ has recently attracted a lot of attention. There are at least two contexts in which this term is used. The first, and probably the more popular, is in the context of Moiré bands [1, 2] in twisted, layered Vanderwaals systems (epitomized by twisted bi-layer Graphene [3–9]) where the multiple band-foldings due to enlarging of the unit-cell results in bands which can have significant regions in the Brillouin zone (BZ) where they disperse very weakly. This leads to an enhanced density of states, and if the chemical potential is around this region, many of the physics of itinerant electrons manifest themselves as a strongly correlated problem as the relevant dimensionless parameter $\nu_F U$ (where ν_F is the density of states at the Fermi surface and U is some scale of interaction in the problem) could be made large even for small U . Another aspect driving the system towards strong correlation physics is the fact that the competition from the kinetic energy (which is characterized by the dispersiveness of a band) falls off due to the reduction of the bandwidth.

The second context in which the term ‘flat band’ is used is in the technically strict sense where systems have perfectly flat dispersionless bands. Some systems that are popularly discussed are the Kagomé lattice [10], the Lieb lattice [11], and the Dice lattice [12]. While there aren’t any natural systems with these specific lattice structures, some of them can be realized in cross-sections of crystals, [13] while some could be artificially engineered [14–18]. It should be noted that these systems have a perfectly flat band within the nearest neighbor (nn) approximation. Beyond the nn, the flatness is disturbed, of course, and the flat band acquires a bandwidth that is generally still much smaller than that of the ‘flat bands’ in the Vanderwaals systems. In this work, we reserve the term ‘flat’ for this second context in the rest of this article.

Investigating flat bands is of fundamental interest [19] for a variety of reasons: it offers novel perspectives on topology [20, 21]; if they are topological, then it is expected that

73 exotic physics of the fractional Quantum Hall effect could be observed in zero-field and at
74 high temperatures [22]; a universal low-energy behavior that is different from the Fermi
75 liquid can be expected as in the theory of the half-filled flat Landau level [23–25]; spin-
76 liquid and chiral spin-liquid behaviors are associated with the presence of a flat energy
77 manifold of excitations and serves as a platform to explore the role of Chern-Simons gauge
78 field [26–30]; the presence of a flat band serves as a possible resolution to the fermion-
79 doubling problem in lattice-based field theories; [31] to name a few. Perhaps the most
80 intriguing yet achievable application of isolated flat band systems would be exploring the
81 physics of the Sachdev-Ye-Kitaev (SYK) model [32–34]: e.g., introducing disorder leads
82 to maximal chaos exhibiting black-hole like behavior (finite entropy at zero temperature)
83 for which there are already various proposals for implementation [35–40]. However, many
84 of these interesting effects only manifest themselves if the flat band is isolated (gapped)
85 from the rest of the system. It is thus desirable to have a design prescription that achieves
86 precisely this.

87 This desire has certainly been recognized by many. Investigation into the existence of
88 the flat band itself revealed that the flat band would be degenerate with dispersive bands,
89 with the degeneracy being protected by topology [41]. It was suggested in Ref. [42] that
90 breaking Time Reversal Symmetry (TRS) was crucial to isolate the flat bands from the
91 dispersive ones by considering staggered fluxes through the unit cell. In a sequence of
92 works [43–45], it was demonstrated that breaking TRS was not necessary, but one would
93 need to fine-tune the system using compact localized states for destructive interference
94 of the electronic states, which would lead to a dispersionless band. There are general
95 considerations from permutation symmetries in graph theory [46] and latent symmetries
96 (associated with destructive interference across certain paths) [47] that can also explain the
97 formation of flat bands on general grounds in general lattices. Certain special symmetry
98 properties of the Hamiltonian (antiunitary-Parity-Time) can also lead to flat bands [48].
99 Reference [49] presented an interesting parameterization of the Kagomé lattice that also
100 successfully isolated the flat band without the consideration of any special symmetries
101 except what the authors identified as inversion [we shall show later (Sec. 5) that it does
102 not have to do much with inversion]. Some works explore the possibility of having a flat
103 band on general grounds, but they either require precise long-ranged hoppings [50] (which
104 is not so desirable in material systems nor in photonic lattices nor ultra-cold atoms) or
105 non-hermitian matrices [51].

106 In this work, we add to the existing body of literature and show that it is possible
107 to have isolated flat bands without breaking TRS, without using long-ranged hopping,
108 without losing hermiticity, and without fine-tuning a system. At this point, we note
109 that very recently in Refs [52, 53], the authors presented a comprehensive analysis on the
110 design of flat bands achieving the same goals of avoiding long-range hopping and fine-
111 tuning. It provides an elegant and robust generalization of our results below, along with
112 the topological classification of these bands. We encourage the reader to refer to this work
113 for a more detailed analysis. While the fundamental requirements for both our works
114 remain similar, we provide an alternative perspective through a focus on providing precise
115 prescriptions to isolate a degenerate flat band and investigate the role of gauge fields in
116 achieving the same. We start from a sufficient condition for the flatband to exist and arrive
117 at a sufficient condition to isolate (gap out) the flatband. The distinguishing feature of our
118 approach is that while the previous works focus on the properties of the Hamiltonian with
119 a flat band, our method involves arriving at flat band systems by performing projections
120 from a ‘parent system.’ In fact, we show that talking about symmetries of the parent
121 system allows for a simpler interpretation of the flat band in the projected systems. To
122 emphasize this point, we first begin with the Kagomé lattice and show that naive attempts

123 to isolate the flat band (via different onsite energies and applying strain) destroy the flat
124 band. However, in addition to already existing prescriptions, we were able to identify
125 another parameterization that preserves the flat band for all ranges of the parameter. But
126 this technique (and the others discussed in the literature) often requires a very specific
127 relationship between various hopping parameters. We then present our main result where
128 we introduce a parent system with certain special properties that guarantees a flat band.
129 And upon performing projections (to be detailed later in the text), we show that the
130 projected systems automatically inherit the various conditions presented earlier for the
131 existence of and isolation of the flat band.

132 We find this condition by first exploring bipartite systems with different system sizes
133 and using the fact that such a system has the number of flat bands equal to the difference in
134 the size of the subsystems [12], thus establishing a sufficient (but not necessary) condition
135 to have flat bands. We then perform a Hilbert-space projection to project out the smaller
136 subsystem, and we show that the larger subsystem will necessarily have flat bands. We
137 explicitly demonstrate that our earlier parameterization of the Kagomé lattice and also
138 some cases discussed earlier in the literature [49] are a special case of this projection
139 prescription.

140 We also identify a symmetry associated with the bipartite system (and not the pro-
141 jected systems), which, when broken, isolates the flat band in the main system and its
142 projected subsystems. We refer to this as a *path-exchange symmetry* with respect to a
143 property which is the set ratios of the paths (in this case hoppings) from different compo-
144 nents of one subsystem to the other. If this set of ratios is the same for two atoms of the
145 larger subsystem, then the whole system is said to have an exchangeable path between
146 the subsystems. We show that the number of exchangeable paths directly controls the
147 degree of degeneracy of the flat band with other dispersive bands. This more fundamental
148 symmetry can map to spatial symmetries like mirror and inversion under special condi-
149 tions and does not necessarily translate to something simple in the projected system and
150 probably explains why there exist so many different attempts to understand the origin of
151 the flat band in various systems. We then relax the bipartite condition in the subsystem
152 that is being projected out and show that our main results still hold.

153 We also apply our prescription to the Lieb and Dice lattices and demonstrate the
154 existence of other lattice structures where flat bands are present and can be isolated by
155 breaking the path-exchange symmetry. In none of these cases where we isolate the flat
156 band do we break time-reversal symmetry as was required in the staggered flux technique
157 of Ref. [42]. Finally, as an application of our prescription, we are able to present scenarios
158 where the hexagonal lattice (such as Graphene) or the chequerboard-like square lattice
159 could also have a flat band. Since our prescription includes carrying out projections from
160 a nn model, we believe that this prescription should be amenable to realization in photonic
161 lattices and circuit QED systems [54–56].

162 As a closing example, we consider the case of a chiral spin-liquid state of fermionized
163 bosons in Kagomé lattice subject to a Chern-Simon’s (CS) field. It was proposed that this
164 state has a flux distribution that would preserve the flat band as opposed to the situation
165 with the regular flux which grows with the area [27]. We apply our results in the presence
166 of a regular Maxwellian flux and show that our projection procedure exactly reproduces
167 the proposed CS flux distribution. The presence of the flat band in such a system was seen
168 as a consequence of the characteristic flux distribution within the unit cell. From our work
169 we now understand that the flat band is actually guaranteed from a more fundamental
170 level.

171 The rest of the text is organized as follows. In Section 2 we introduce the Kagomé
172 lattice and show that the common ideas to modify the lattice ends up disturbing the flat

173 band. In Section 3, we introduce our parameterization that preserves the flat band and
 174 discuss the physical meaning of the parameterization. In Section 4 we introduce the pro-
 175 jection prescription in terms of bi-partite systems to generate flat bands. In Section 5 we
 176 identify the path-exchange symmetry in our bi-partite systems, which upon being broken,
 177 isolates the flat band. We then show that the bipartite condition is not a strict require-
 178 ment. In Section 6, we demonstrate all of the above ideas in the Lieb and Dice lattices.
 179 In Section 7, we demonstrate why the proposed Chern-Simons type flux distribution on
 180 a Kagomé lattice guarantees a flat band, whereas the usual Maxwellian flux distribution
 181 does not. Finally, we summarize our results in Section 8. The Appendix includes some
 182 details and proofs that did not find their place in the main text.

183 2 Kagomé: naïve attempts to lift the flat band degeneracy

184 We start by considering the Hamiltonian for the Kagomé lattice within a tight-binding
 185 model with only nn hoppings:

$$H_{\text{Kg}} = -t \begin{pmatrix} 0 & 1 + e^{-i\vec{k}\cdot\vec{R}_1} & 1 + e^{-i\vec{k}\cdot\vec{R}_2} \\ 1 + e^{i\vec{k}\cdot\vec{R}_1} & 0 & 1 + e^{-i\vec{k}\cdot\vec{R}_3} \\ 1 + e^{i\vec{k}\cdot\vec{R}_2} & 1 + e^{i\vec{k}\cdot\vec{R}_3} & 0 \end{pmatrix}, \quad (1)$$

186 where t is the nn hopping matrix element, $\vec{R}_1 = (1, 0)$, $\vec{R}_2 = (\frac{1}{2}, \frac{\sqrt{3}}{2})$ are the translation
 187 vectors of the lattice, $\vec{R}_3 = \vec{R}_2 - \vec{R}_1$, and \vec{k} is the Bloch momentum in the first Brillouin zone
 188 (fBZ) and is made dimensionless by absorbing the lattice constant a . This Hamiltonian
 189 is written in the basis $\hat{\Psi}_{\vec{k}} = (\hat{c}_{\vec{k},A}, \hat{c}_{\vec{k},B}, \hat{c}_{\vec{k},C})^T$, where A, B, C are the three atoms within
 190 the unit cell [see Fig. 1(a)]. The spectrum contains a flat band as shown in Fig. 1(b).

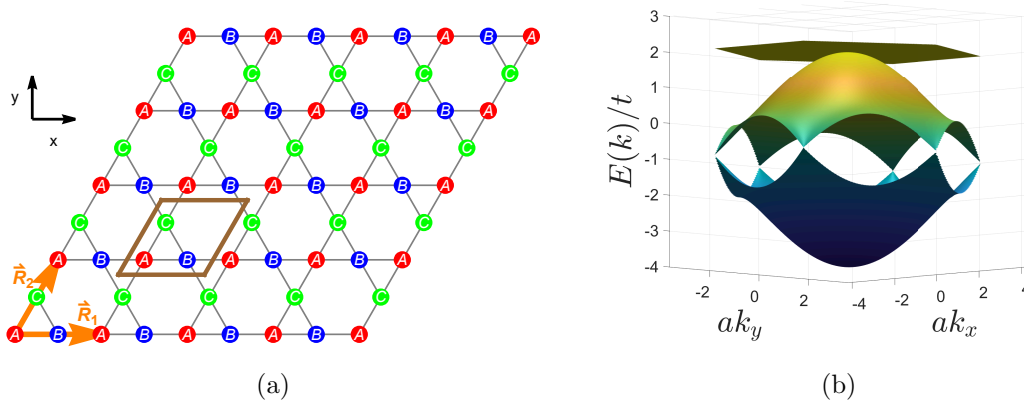


Figure 1: (a) Kagomé lattice with three atoms A, B, C in the unit cell and the translation vectors \vec{R}_1 and \vec{R}_2 . The brown parallelogram is a unit cell (b) The energy spectrum for the Kagome lattice. Note the presence of the flat band that is degenerate with the dispersing middle band at the Γ -point $(0,0)$.

191 In order to lift the degeneracy at the Γ -point, one could envision multiple ways to
 192 perturb the system: break the similarity of A, B, C (sub-lattice symmetry), break or lower
 193 some translational or point-group symmetry, or break Time-reversal symmetry (TRS). We
 194 shall briefly demonstrate below that while the standard ways to apply these perturbations

195 may lift the degeneracy at the Γ -point, they also destroy the flatness of the band. Further,
 196 the degeneracy point sometimes just gets moved to other points in the fBZ.

197 2.1 Onsite perturbations and strain

198 Consider first making the three atoms different by subjecting them to different on-site
 199 potentials. To model this, one could add the following term to the Hamiltonian: $\delta H_{\text{site}} =$
 200 $-t \text{Diag}(0, \Delta, -\Delta)$. For $\Delta \ll 1$, the Γ -point eigenvalues are $t \left(2 \pm \frac{\Delta}{\sqrt{3}}\right) + \mathcal{O}(\Delta^2)$ and $-4t +$
 201 $\mathcal{O}(\Delta^2)$. However, as seen in Fig. 2(a), numerical diagonalization shows that this condition
 202 just splits the quadratic Γ -point degeneracy to two Dirac points. So the degeneracy of the
 203 bands is not really lifted. This also destroys the flat band.

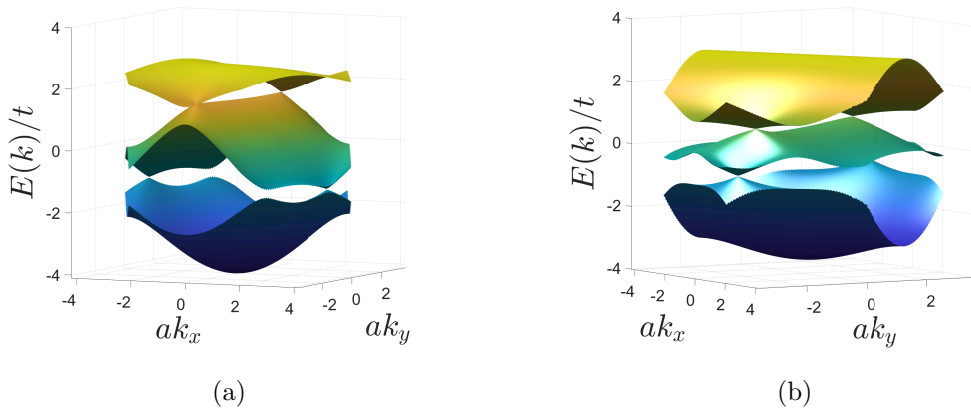


Figure 2: (a) Spectrum for the Kagomé system with different onsite energies ($\Delta = 0.5$). The Γ -point degeneracy is lifted, but it splits into two Dirac points at different k values. The flatness of the flat band is also lost. (b) Spectrum for Kagomé lattice under a uniaxial strain along the diagonal that intersects the $B - C$ bond in Fig. 1a. Once again, the flat band is lost. Here $\delta t = 0.5$.

204 One can also consider modeling the effect of the strain. For simplicity, consider a
 205 uniaxial strain applied to the system. This would have two effects on the system: alter
 206 the translation vectors and alter the hoppings. The change in translation vectors will only
 207 act as a change in “gauge” in the k -space [57–60] and hence not really alter the qualitative
 208 aspects of the spectrum. The change in hoppings alters the symmetry properties of the
 209 3×3 Bloch Hamiltonian. For the orientation shown in Fig. 1(a), applying a strain along
 210 the diagonal that intersects the $B - C$ bonds would result in the following Hamiltonian:

$$H_{\text{Kg, strain}} = - \begin{pmatrix} 0 & (t - \delta t)(1 + e^{-i\vec{k} \cdot \vec{R}_1}) & (t - \delta t)(1 + e^{-i\vec{k} \cdot \vec{R}_2}) \\ (t - \delta t)(1 + e^{i\vec{k} \cdot \vec{R}_1}) & 0 & (t + \delta t)(1 + e^{-i\vec{k} \cdot \vec{R}_3}) \\ (t - \delta t)(1 + e^{i\vec{k} \cdot \vec{R}_2}) & (t + \delta t)(1 + e^{i\vec{k} \cdot \vec{R}_3}) & 0 \end{pmatrix} \quad (2)$$

211 The full spectrum plotted in Fig. 2(b) shows that the flat band is lost. Moreover, the
 212 quadratic touching point shifts away from the Γ -point as it splits into two Dirac points.
 213 This splitting of the Γ -point degeneracy into Dirac points is the same phenomenon that
 214 was discussed in Refs. [61, 62], although not in the context of strain.

215 2.2 Breaking TRS

216 In another attempt to lift the degeneracy of the flat band, we may also consider breaking
 217 TRS by applying an out-of-plane magnetic field to the system. Since we are working within

218 a spin-less model, the only effect of the magnetic field would be the orbital effect. We
 219 address this by constructing a Hofstadter model for the Kagome lattice (see, e.g. [63]. In
 220 Fig. 3 we show, as a representative case, the spectrum for a flux per unit cell of $\pi\phi_0$ (where
 221 $\phi_0 = \frac{h}{e}$ is the single electron flux quantum) and that the flat band becomes dispersive.
 222 There are, however, ways to break TRS and still preserve the flat band. This requires
 223 using staggered flux as introduced in Ref. [42] or a Chern-Simons flux (which is focused
 224 through one part of the unit cell) like in Ref. [27], and we shall not dwell on this point as
 225 it is beyond the scope of this work.

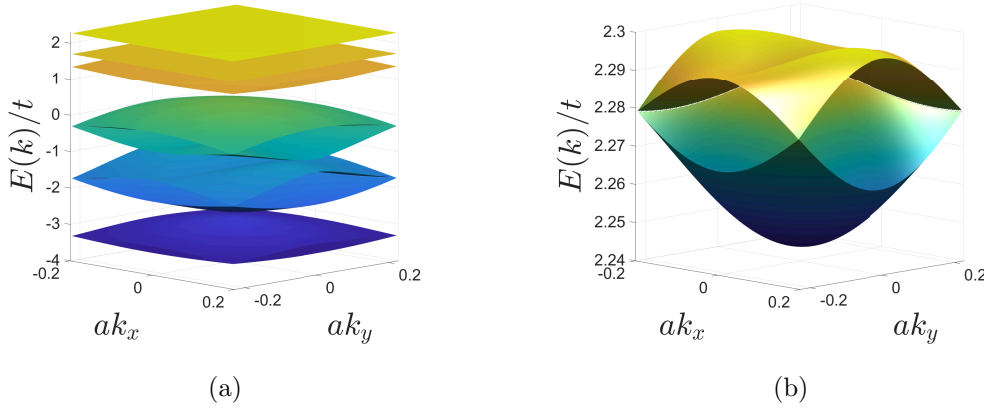


Figure 3: (a) Energy bands of the Kagomé lattice with $\pi\phi_0$ flux distributed uniformly in the unit cell. (b) A zoomed-in version of the top bands showing the dispersive nature. This remains true for any other uniform flux linked to the unit cell.

226 3 Kagomé: Flat band preserving parameterization

227 While it seems that any perturbation we apply to the system lifts the flatness of the band,
 228 one may wonder if there could be a parameterization that preserves the flatness of the
 229 band. To tackle this question, let us consider the Kagomé Hamiltonian in the generic form

$$\mathcal{H} = -t \begin{pmatrix} 0 & \alpha_1 & \alpha_2 \\ \alpha_1^* & 0 & \alpha_3 \\ \alpha_2^* & \alpha_3^* & 0 \end{pmatrix}. \quad (3)$$

230 The eigenvalues are the roots of the equation:

$$-(E/t)^3 + (E/t) (|\alpha_1|^2 + |\alpha_2|^2 + |\alpha_3|^2) - 2\text{Re}[\alpha_1^* \alpha_2 \alpha_3^*] = 0. \quad (4)$$

231 To have a flat band at $E/t = f$ (independent of \vec{k}), we necessarily need the \vec{k} -dependence
 232 of α_i to be such that for all $\vec{k} \in \text{fBZ}$

$$|\alpha_1|^2 + |\alpha_2|^2 + |\alpha_3|^2 = \frac{2\text{Re}[\alpha_1^* \alpha_2 \alpha_3^*]}{f} + f^2. \quad (5)$$

233 In fact, if such a flat band were to exist, then Eq. (5) would have to be satisfied for some
 234 real value of f . Plugging this into the characteristic equation leads us to

$$-(E/t)^3 + (E/t) \left(\frac{A}{f} + f^2 \right) - A = 0, \quad (6)$$

235 where $A \equiv 2\text{Re}[\alpha_1^* \alpha_2 \alpha_3^*]$. The eigenvalues would then be

$$\begin{aligned} E_0 &= tf; \\ E_+ &= \frac{tf}{2} \left(-1 + \sqrt{1 + 4A/f^3} \right); \\ E_- &= \frac{tf}{2} \left(-1 - \sqrt{1 + 4A/f^3} \right). \end{aligned} \quad (7)$$

236 However, if there exists no such f , then the above expressions are no longer the solution.
 237 One could then ask what are the conditions for which f could exist or equivalently, under
 238 what conditions would Eq. (5) be satisfied. Note that this equation presents one constraint
 239 on the parameters of this equation which are α_i ($i \in \{1, 2, 3\}$). At this stage, it might seem
 240 like one should always be able to satisfy this. However, note that the α_i 's are, in turn,
 241 functions of k_x, k_y and f . The k_i 's are subject to the condition that they must be bound
 242 to the fBZ. But given that the k_i 's appear as arguments of periodic functions, this bound
 243 is not really an additional constraint. But, the α_i 's themselves are not independent. In
 244 fact, the Kagomé Hamiltonian's structure ensures that $(\alpha_1 - 1)^*(\alpha_2 - 1) = \alpha_3 - 1$, which
 245 are two more constraints on the parameters. Thus, we have a situation with 3 constraints
 246 and 3 parameters. Since they are not linear, they may or may not be satisfied in general.

247 For completeness, we could ask if any of the dispersive bands (E_{\pm}) could intersect the
 248 flat band E_0 . Setting them equal to each other immediately establishes that for real values
 249 of A and f , only E_+ could intersect with E_0 and this would happen at those \vec{k} -points where

$$2\text{Re}[\alpha_1^* \alpha_2 \alpha_3^*] \equiv A = 2f^3. \quad (8)$$

250 In fact, for the case of the Kagomé lattice, we note that $\alpha_i = 1 + e^{-i\vec{k} \cdot \vec{R}_i}$ and Eq. (5) is
 251 satisfied for $f = 2$ and for all \vec{k} , establishing the condition for the flat band. Further, Eq.
 252 (8) is also satisfied only at the Γ -point indicating that the flat band would be degenerate
 253 with the dispersive band at the Γ -point.

One may now wonder if there are other scenarios, other than the Kagomé lattice,
 where Eq. (5) could be satisfied. The answer is affirmative and a family of scenarios
 is presented below. Consider the modification where α_i is changed from $1 + e^{-i\vec{k} \cdot \vec{R}_i}$ to
 $(1 + r) + (1 - r)e^{-i\vec{k} \cdot \vec{R}_i}$, with $|r| < 1$. The physical meaning of the r -parameter will be
 discussed in a subsequent section. In fact, one could factor out $1 + r$ and absorb it into
 the hopping element t yielding the following transformation $t \rightarrow \tilde{t} = t(1 + r)$, and

$$\alpha_i \rightarrow \tilde{\alpha}_i = 1 + \frac{1 - r}{1 + r} e^{-i\vec{k} \cdot \vec{R}_i} = 1 + e^{-i\vec{k} \cdot \vec{R}_i - h},$$

where h is defined through the equation $r = \tanh \frac{h}{2}$. This allows us to express

$$\tilde{\alpha}_i = 2 \cos \left(\frac{\vec{k} \cdot \vec{R}_i}{2} - \frac{ih}{2} \right) e^{-i\frac{\vec{k} \cdot \vec{R}_i}{2} - \frac{h}{2}}.$$

254 From these definitions, we observe that the flat band condition of Eq. (5)

$$\sum_{i=3} |\tilde{\alpha}_i|^2 = \frac{2\text{Re}[\tilde{\alpha}_1^* \tilde{\alpha}_2 \tilde{\alpha}_3^*]}{f} + f^2 \quad (9)$$

255 can now be satisfied with $f = 2e^{-\frac{h}{2}} \cosh \frac{h}{2}$ (see Appendix A for details). The spectrum
 256 is given by Eq. (7) but with $\alpha_i \rightarrow \tilde{\alpha}_i$ and $t \rightarrow \tilde{t}$. The condition for band-touchings also
 257 remains the same as Eq. (8) but with $\alpha_i \rightarrow \tilde{\alpha}_i$. A direct evaluation shows that if the

258 condition is satisfied for α_i , then it is automatically satisfied for $\tilde{\alpha}_i$. This means that the
 259 flat band remains flat at $E = \tilde{t}f = 2\tilde{t}e^{-\frac{h}{2}} \cosh \frac{h}{2} = 2t$. The introduction of the parameter
 260 r neither lifts nor moves the degeneracy at the Γ -point. In fact, observe that when $r \rightarrow 0$,
 261 $\tilde{\alpha}_i \rightarrow \alpha_i$, and the formulae smoothly connect to the original Kagome lattice. Thus, we
 262 have a family of flat band systems characterized by the parameter r .

263 The spectra for the modified lattices are shown in Fig. 4 for various values of r . As
 264 observed above, for any value of r , the flat band is preserved. Although the Dirac point at
 265 the K and K' points of the fBZ are gapped out, the r parameter preserves the degeneracy
 266 at the Γ -point consistent with the analysis above.

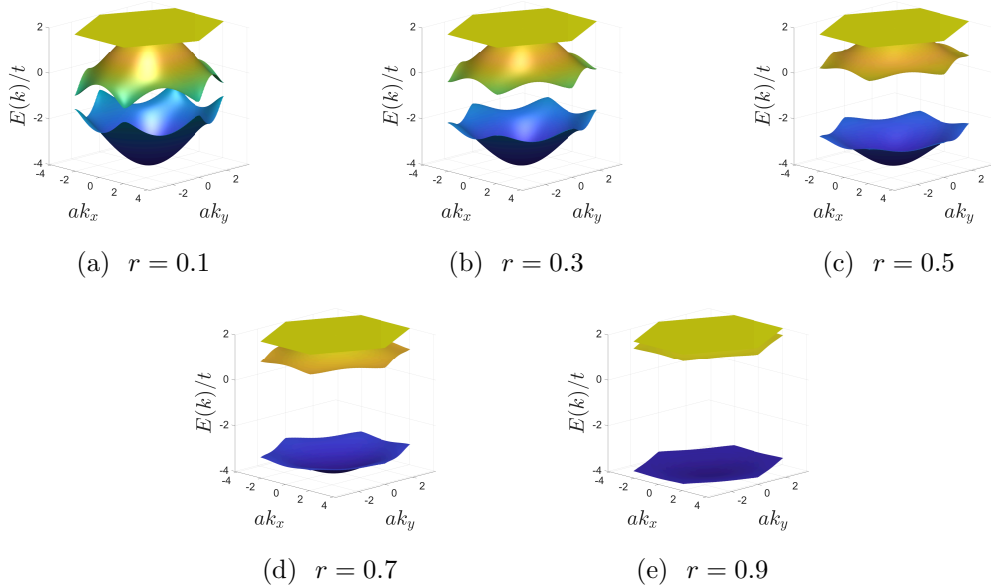


Figure 4: Evolution of the spectrum for the Kagomé lattice with the parameter r . The flat band is located at $E = \tilde{t}f = 2t$. As r increases, the Dirac points gap out, but the flat band maintains a quadratic band touching with the dispersive band. As $r \rightarrow 1$, the dispersive band merges with the flat band. The spectrum remains the same under $r \rightarrow -r$.

267 3.1 Physical meaning behind the r -parameter

268 The introduction of the r parameter allowed for the same parameterization of the flat band
 269 condition as the original Kagome lattice but with a modified (complex) phase. Further,
 270 this parameterization also allows us to interpret $t(1+r)$ as hopping within the unit cell
 271 and $t(1-r)$ and hopping outside the unit cell (because this is the term in the Bloch
 272 Hamiltonian associated with the translation phase factor). For $r > 0$, it would correspond
 273 to bringing the 3 atoms closer together (without altering the lattice constant) towards one
 274 corner of the unit cell, as shown in Fig. 5. For $r < 0$ the deformation takes the atoms
 275 toward the other corner of the unit cell. This deformation is analogous to the ‘breathing’
 276 anisotropy considered in frustrated Kagomé lattices [64]. Further, the case with $r > 1$
 277 corresponds to negative t_{inter} , which is equivalent to having a π phase attached to the
 278 hopping element. This case will be discussed in more detail in the next subsection.

279 Observe from Fig. 5 that when $r = 1$, the intercell hopping $t(1-r) = 0$ (molecular
 280 limit) and we do not hop to the neighboring unit cells and thus we get a non-dispersive
 281 3-level system. Because of the non-dispersive nature, the bands are trivially flat, and two
 282 of them are degenerate because we are still satisfying Eq. (8) for touching of the flat

283 band with one other band. For $r < 0$, we effectively swap intercell and intracell hoppings.
 284 This just amounts to mirroring the unit cell about a diagonal and thus does not change
 285 anything in the spectrum.

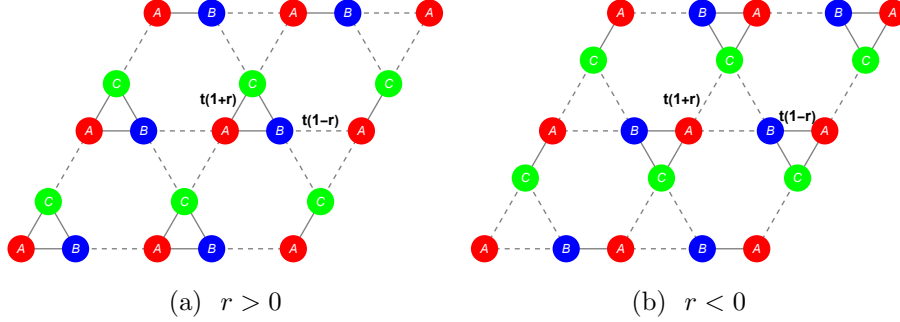


Figure 5: Modified Kagomé lattice. For $r > 0$, the basic modification is such that it brings the atoms together towards one corner of the unit cell. For $r < 0$ the atoms are moved closer toward the other corner of the unit cell. The original Kagomé lattice is restored at $r = 0$.

286 3.2 Model with $|r| > 1$

287 When $|r| > 1$ one of either the inter-cell hopping or the intra-cell hopping parameters
 288 goes negative. From a solid-state point of view, this is clearly unphysical, however, we
 289 still have a well-defined spectrum and eigenfunctions. One could imagine the bonds with
 290 negative hopping to be associated with a phase of π . In Fig. 6 (a) we show the resulting
 291 flux distribution. This is clearly a 2π -flux per unit cell, but the flux is modulated within
 292 the unit cell such that the flux is concentrated in the hexagonal region and one of the
 293 two triangular regions in the unit cell. This could be viewed as the flux through the
 294 closed structure in the unit cell (the triangle ABC) having zero flux, and the flux is only
 295 “in between” these closed structures. In the limit $r \rightarrow \infty$ (recall that the energy of the
 296 flat band is independent of r) the lattice returns to the Kagomé form factor, albeit with
 297 the modified flux. Although there is flux distribution within the unit cell, TRS is still
 298 preserved because the phase is π which is the same as $-\pi$. In fact, this is exactly one of
 299 the cases arrived at in Ref. [42] but is naturally included in our parameterization.

300 The spectrum for $|r| > 1$ is shown in Fig. 6 (b). As discussed in an earlier subsection,
 301 at $r = 1$, the dispersing band merges with the original flat band. However, as r becomes
 302 greater than 1, the dispersing band moves above the flat band. This is an interesting
 303 example where one band completely passes through another one. Note also that the
 304 Γ -point remains degenerate.

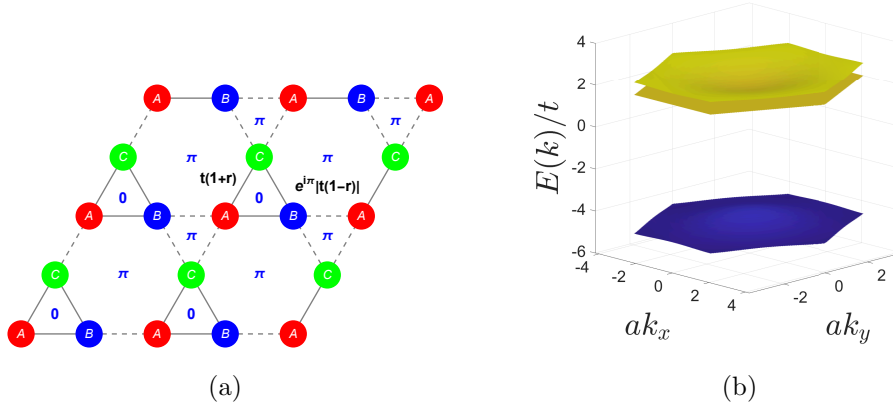


Figure 6: (a) Modified Kagomé lattice for $r > 1$. The negative hopping could be seen as the bond having a π -phase that results in characteristic 2π -flux distribution per unit cell as shown. (b) The energy spectrum for $r = 1.2$. The flat band is preserved and so is the degeneracy at the Γ -point. However, note that the dispersive band is now above the flat band.

305 Another application of models with $|r| > 1$ would be in scenarios where a coupled
 306 system of oscillators is mapped to the tight-binding model. This is realizable in photonic-
 307 crystal systems and even in cold atom systems. Thus, we have demonstrated that there
 308 exists a parameterization in terms of the change of the basis of the unit-cell, mathemati-
 309 cally realized by introducing the parameter r , that preserves the flat band. At this stage,
 310 this is just one additional means to discuss the condition for flat bands. However, we shall
 311 now describe a prescription to generate flat bands on general grounds, which includes all
 312 the cases discussed above (and in the literature).

313 4 A prescription to generate flat band systems

314 In the previous sections, we presented a detailed analysis of the Kagomé system and its
 315 modifications that would preserve the flat band. The approach was rather direct where
 316 we searched for the parameters that would keep a band dispersionless (\vec{k} -independent).
 317 This approach, however, is not generalizable to investigate other systems as they would
 318 have to be dealt with on a case-by-case basis. However, the presence of the flat band in
 319 the Kagomé lattice could be deduced in a rather interesting manner. Consider a bipartite
 320 system as shown in Fig. 7 with 2 and 3 atoms per unit cell and hoppings only between
 321 the respective subsystems: consisting of X, Y atoms and A, B, and C atoms.

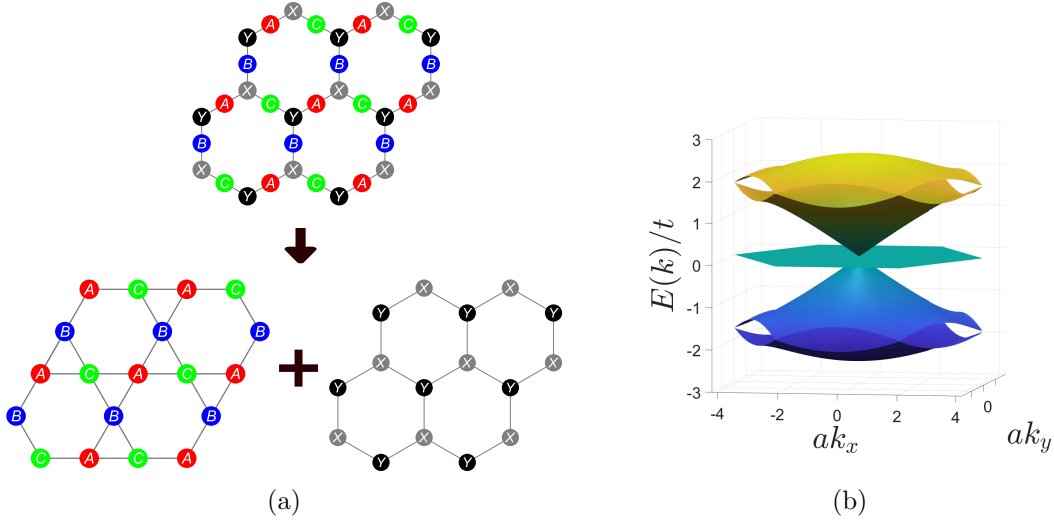


Figure 7: (a) Bipartite system with 2 and 3 atoms per unit cell. (b) The energy spectrum for the 5 atoms per unit cell structure is particle-hole symmetric. This is guaranteed by the bipartite nature of the system.

322 The Hamiltonian is given by

$$H_5 = -t \begin{pmatrix} 0 & 0 & 1 & 1 & 1 \\ 0 & 0 & 1 & e^{-i\vec{k}\cdot\vec{R}_1} & e^{-i\vec{k}\cdot\vec{R}_2} \\ 1 & 1 & 0 & 0 & 0 \\ 1 & e^{i\vec{k}\cdot\vec{R}_1} & 0 & 0 & 0 \\ 1 & e^{i\vec{k}\cdot\vec{R}_2} & 0 & 0 & 0 \end{pmatrix}, \quad (10)$$

323 where the basis is $\hat{\Psi}_{\vec{k}} = (\hat{c}_{\vec{k},X}, \hat{c}_{\vec{k},Y}, \hat{c}_{\vec{k},A}, \hat{c}_{\vec{k},B}, \hat{c}_{\vec{k},C})^T$. There is a well known property of
 324 a bipartite Hamiltonian, $H_{(n+m)\times(n+m)}$ (of subsystem sizes n and m), one can always
 325 construct the matrix $\mathcal{C} \equiv \text{Diag}(1_{n\times n}, -1_{m\times m})$ such that $\{\mathcal{C}, H\} = 0$ (i.e. it anti-commutes
 326 with the Hamiltonian). This implies that for every state with energy E , there must
 327 exist another orthogonal state at energy $-E$. This is commonly known as a particle-hole
 328 symmetric spectrum. Fig. 7(b) shows the numerically evaluated spectrum for H_5 . It is
 329 easy to argue from this property that if $m+n$ is odd, we need to have a state at $E=0$
 330 and thereby guaranteeing a flat band [12]. However, we wish to show that there is a more
 331 fundamental reason for having flat bands which goes beyond this standard argument.

Starting from a bipartite system, consider projecting out one subsystem, by using the
 Löwdin's method [65], at some energy scale of interest E_0 . This is a method that projects
 out one subspace from the system and the scale E_0 plays the role of chemical potential in
 most cases. Let us suppose that we would like to project out the subsystems A, B, and C
 and express the Hamiltonian purely in terms of the states of the other subsystems X, Y.
 To apply the Löwdin's method, first view the Hamiltonian H_5 as blocks

$$\begin{pmatrix} [H_{GG}]_{2\times 2} & [H_{GK}]_{2\times 3} \\ [H_{KG}]_{3\times 2} & [H_{KK}]_{3\times 3} \end{pmatrix}.$$

332 Then, the effective Hamiltonian projected onto the G space (consisting of X,Y) would be

$$H_{\text{eff},G}(E_0) = H_{GG} + H_{GK}[E_0 - H_{KK}]^{-1}H_{KG}. \quad (11)$$

333 Because of the bipartite nature with $K \rightarrow$ Kagomé and $G \rightarrow$ Graphene, $H_{GG} = 0$ and
 334 $H_{KK} = 0$. This yields

$$H_{\text{eff},G}(E_0) = \frac{H_{GK}H_{KG}}{E_0}. \quad (12)$$

335 Similarly, the effective Hamiltonian projected onto the K space is

$$H_{\text{eff},K}(E_0) = \frac{H_{KG}H_{GK}}{E_0}. \quad (13)$$

336 Usually, Löwdin's method is used in the perturbative sense at some energy scale that
 337 separates out the states far away from that energy scale. However, due to the bipartite
 338 nature, we can perform an exact projection, as outlined above. There are two observations
 339 of interest for the Hamiltonians $H_{\text{eff},G}$ and $H_{\text{eff},K}$:

340 1. We can recognize

$$H_{\text{eff},G} = \frac{t^2}{E_0} \begin{pmatrix} 3 & 1 + e^{i\vec{k}\cdot\vec{R}_1} + e^{i\vec{k}\cdot\vec{R}_2} \\ 1 + e^{-i\vec{k}\cdot\vec{R}_1} + e^{-i\vec{k}\cdot\vec{R}_2} & 3 \end{pmatrix} \quad (14)$$

341 as the Hamiltonian for Graphene and

$$H_{\text{eff},K} = \frac{t^2}{E_0} \begin{pmatrix} 2 & 1 + e^{-i\vec{k}\cdot\vec{R}_1} & 1 + e^{-i\vec{k}\cdot\vec{R}_2} \\ 1 + e^{i\vec{k}\cdot\vec{R}_1} & 2 & 1 + e^{-i\vec{k}\cdot\vec{R}_3} \\ 1 + e^{i\vec{k}\cdot\vec{R}_2} & 1 + e^{i\vec{k}\cdot\vec{R}_3} & 2 \end{pmatrix} \quad (15)$$

342 as the Hamiltonian for the Kagomé lattice. This could have been expected since the
 343 second order hops connects each subsystem to itself.

344 2. Note that $H_{KG} = H_{GK}^\dagger$. A non-square matrix M has the property that $M^\dagger M$ and
 345 MM^\dagger , which are of different ranks, share the same eigenvalues, with additional zeroes
 346 making up for the difference in ranks (see Appendix B). Thus, our two subsystems
 347 will be such that $H_{\text{eff},K} \sim H_{KG}H_{GK}$ will have the *same eigenvalues* as $H_{\text{eff},G} \sim$
 348 $H_{GK}H_{KG}$ but an additional 0 due to the rank mismatch. This zero is \vec{k} independent
 349 and hence results in a flatband. This is the more fundamental reason behind the
 350 formation of flat bands and most other conditions, if not all, are derivable from this
 351 construction. We demonstrate a few other cases later in this article.

352 This explains why the Kagomé lattice spectrum has a flat band and also why the rest of
 353 the spectrum is exactly the same as Graphene.

From point (2) above, we can conclude a general rule that if one constructs a bipartite system, projecting out the smaller subsystem will result in a flat band in the new effective system. The generality of the prescription outlined above implies that the detailed structure (the dimensions or even the matrix elements) of H_{GK} does not matter. In fact, our r parameterization is a special case of this general rule. To demonstrate this point, consider first, the H_5 Hamiltonian for the original Kagomé and Graphene lattices. Here

$$H_{GK} = -t \begin{pmatrix} 1 & 1 & 1 \\ 1 & e^{-i\vec{k}\cdot\vec{R}_1} & e^{-i\vec{k}\cdot\vec{R}_2} \end{pmatrix}.$$

This can be generalized to

$$H_{GK} = - \begin{pmatrix} t_{G_1K_1} & t_{G_1K_2} & t_{G_1K_3} \\ t_{G_2K_1} & t_{G_2K_2}e^{-i\vec{k}\cdot\vec{R}_1} & t_{G_2K_3}e^{-i\vec{k}\cdot\vec{R}_2} \end{pmatrix}$$

354 and the flat band would still persist owing to the size mismatch of the two subsystems.
 355 The r parameterization (and all of the ensuing discussion) corresponds to the choice of
 356 $t_{G_1K_i} = \sqrt{t(1+r)}$ and $t_{G_2K_i} = \sqrt{t(1-r)}$, for $i \in \{1, 2, 3\}$, and hence preserves the
 357 flat band. We emphasize that the prescription we provide (based on bi-partiteness) is a
 358 *sufficient* condition to get a flat band but not a necessary one.

359 4.1 Flat bands beyond the bipartite condition

360 A bipartite system with different system sizes having a flat band is a rather straightforward
 361 result. However, we now wish to show that this condition is not necessary. We can start
 362 from the bipartite system and then allow for hoppings or energies in the subsystem to be
 363 projected out. This would still guarantee the presence of the flat band (the particle-hole
 364 symmetry will no longer persist, of course) in the parent system and also in the projected
 365 subsystem (with the larger size). The existence of the flat band is controlled solely by the
 366 existence of the non-square coupling matrix between a subsystem that does not talk to
 367 itself and another subsystem with a smaller size.

To see this, let us first note that the effective Hamiltonian now goes from

$$H_{KG}H_{GK} \rightarrow H_{KG}[E_0 - H_{GG}]^{-1}H_{GK},$$

where H_{GG} is an arbitrary matrix. The matrix $E_0 - H_{GG}$ can be diagonalized as $M\Lambda M^\dagger$, where Λ is the diagonal matrix of the eigenvalues of H_{GG} and M is the matrix of eigenvectors of H_{GG} . Thus, $[E_0 - H_{GG}]^{-1} = M[E_0 - \Lambda]^{-1}M^\dagger$. This allows us to write

$$H_{KG}[E_0 - H_{GG}]^{-1}H_{GK} = \underbrace{H_{KG}M}_{\tilde{H}_{KG}}[E_0 - \Lambda]^{-1}\underbrace{M^\dagger H_{GK}}_{\tilde{H}_{GK}}.$$

368 Due to Hermiticity we have $H_{GK} = H_{KG}^\dagger$ and this implies $\tilde{H}_{GK} = \tilde{H}_{KG}^\dagger$. Thus, we
 369 arrive at the form $[\tilde{H}_{KG}]_{ac}D_{cd}[\tilde{H}_{GK}]_{db}$, where $D_{ab} = d_a\delta_{ab}$ is a diagonal matrix. Since,
 370 $\tilde{H}_{KG} = \tilde{H}_{GK}^\dagger$, the above product can be written as $[\tilde{H}_{KG}]_{ac}[\tilde{H}_{GK}]_{cb}$, where $[\tilde{H}_{KG}]_{ab} =$
 371 $[\tilde{H}_{KG}]_{ab}\sqrt{d_a}$. Since this maintains $\tilde{H}_{KG} = \tilde{H}_{GK}^\dagger$, we can map this non-bipartite system to
 372 a strict bipartite system and apply all the same arguments: the size mismatch of the two
 373 systems would result in a zero eigenvalue and hence a flat band. In this sense, we only need
 374 the bipartiteness to choose the subsystems and then allow the smaller subsystem to have
 375 any hoppings and the resulting system would still have a flat band. We demonstrate this
 376 in Fig. 8 where we include the off-diagonal elements in H_{GG} as $t'(1 + 0.1e^{i\vec{k}\cdot\vec{R}_1} + 0.5e^{i\vec{k}\cdot\vec{R}_2})$
 377 and its c.c with $t' = 0.5E_0$ (this simply accounts some hoppings in the GG subspace). The
 378 particle-hole symmetry is lost, but the flat band still exists.

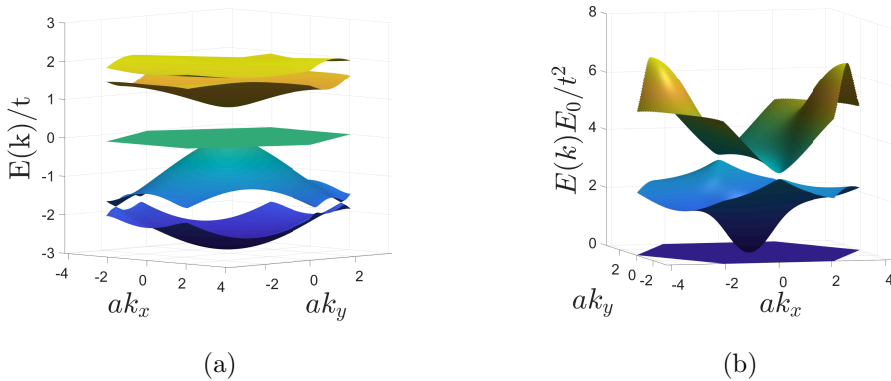


Figure 8: (a) The spectrum of the H_5 system still has a flat band with $H_{GG} \neq 0$ (but $H_{KK} = 0$), which is in violation of the bipartite condition. (b) The flat band in the projected subsystem

379 Lastly, we show that deviation from the stated condition above destroys the flat band.
 380 Consider the simple case of adding different onsite energies to the sites of the subsystem

381 of interest. Consider

$$H_{KK} = \begin{pmatrix} E_a & 0 & 0 \\ 0 & 0 & 0 \\ 0 & 0 & 0 \end{pmatrix}.$$

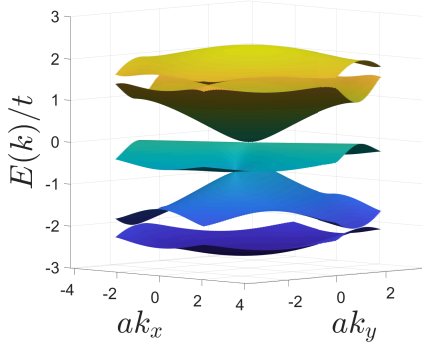
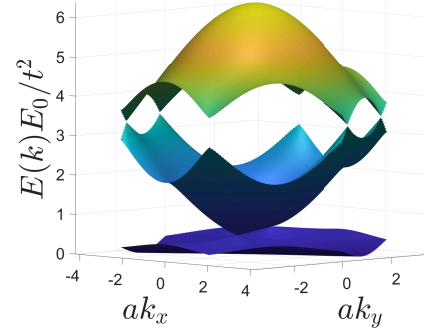
382 The spectrum for such a case is shown in Fig. 9(a) and the ensuing projected system also
 383 shown in (b) also loses the flatness. As another example for demonstrating that violating
 384 the stated condition destroys the flatness, consider the strained Hamiltonian in Eq. (2)
 385 which does not have a flat band. This is so because arriving at this form from the H_5
 386 formulation requires choosing

$$H_{KK} = \begin{pmatrix} 0 & c_1 & c_2 \\ c_1^* & 0 & c_3 \\ c_2^* & c_3^* & 0 \end{pmatrix} \quad (16)$$

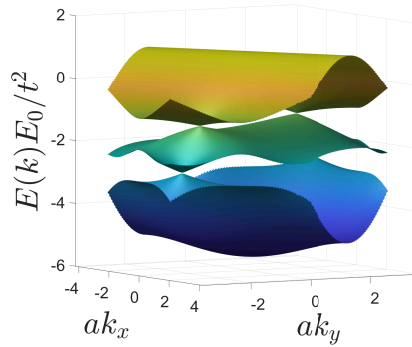
387 with $c_1 = -\frac{t\delta t}{E_0}(1 + e^{-i\vec{k}\cdot\vec{R}_1})$, $c_2 = -\frac{t\delta t}{E_0}(1 + e^{-i\vec{k}\cdot\vec{R}_2})$, $c_3 = \frac{t\delta t}{E_0}(1 + e^{-i\vec{k}\cdot\vec{R}_3})$. This violates
 388 our stated condition that H_{KK} still needs to be of the ‘bipartite’ nature. Indeed after
 389 Löwdin’s projection we get

$$H_{\text{eff}} = H_{\text{eff},K} + H_{KK}, \quad (17)$$

390 where $H_{\text{eff},K}$ is the same as in Eq. (15). This is nothing but the strained Hamiltonian of
 391 Eq (2), with an overall scale factor of $\frac{t}{E_0}$. The spectrum is shown in Fig. 9(c). Physically
 392 including c_i amounts to including nnn terms in the H_5 system.


 (a) H_5 with onsite energy


(b) Projected Kagomé with on-site energy



(c) Projected Kagomé with non-bipartite terms

Figure 9: (a) The energy spectrum for the H_5 system with an on-site energy $E_a = t$. (b) The spectrum after projection from the H_5 system onto the ABC subsystem. (c) The spectrum after projection from the H_5 system with the non-bipartite terms added to the ABC subsystem. Here, $\delta t = 0.5t$. In both cases, (b) and (c), the loss of our stated flat band condition indeed results in the loss of the flat band.

393 5 Isolating the flat band

394 Having formulated a technique to generate a family of flat band systems, we note that
 395 in the cases we looked at, the flat band always appeared degenerate with a dispersive
 396 band. However, if we let $t_{G_i K_j}$ to be different from each other, we preserve the flat
 397 band (since any change within the matrix H_{GK} is allowed) as well as isolate it from the
 398 dispersive band. As an example, consider the case where we displace one of the $a, b,$
 399 or c atoms such that it is closer to x and further from y in Fig. 10(b) such that with
 400 $t_{G_1 K_1} = t_{G_1 K_2} = t_{G_2 K_1} = t_{G_2 K_2} = t, t_{G_2 K_3} = t + \delta t$ and $t_{G_1 K_3} = t - \delta t$. After projecting
 401 the system onto the Kagomé form, an explicit calculation shows that the gap at the Γ -point
 402 is $\frac{\delta t^2}{3t}$ (for $\delta t \ll t$).

403 **The path-exchange symmetry** The above change falls under case shown in Fig.
 404 10(d). This differs from the cases in Fig. 10(a), (b), and (c) in the following way. Con-
 405 sider the sets of paths taking us from the larger subsystem (ABC) to the smaller (XY):
 406 $\{AX, AY\}, \{BX, BY\}, \{CX, CY\}$. Consider the set $\{r_X^{AB}, r_Y^{AB}\}$ created from the ratios
 407 $r_X^{AB} \equiv \frac{AX}{BX}$ and $r_Y^{AB} \equiv \frac{AY}{BY}$. The elements of this set correspond to the ratio of paths-

408 to-other-subsystem between two atoms of the larger subsystem. Special situations arise
 409 when all the entries of the set are identical (i.e., can be reduced to a unit set). When
 410 we find a pair AB where the set of ratios could be reduced to a unit set, then we say we
 411 have a path-exchange in the system (physically, the presence of a unit set between pairs of
 412 atoms means that the paths to hop across subsystems are exchangeable between these two
 413 atoms). We show in Appendix C that for a bipartite system (of size m, n with $m > n$),
 414 the presence of r such path-exchanges leads to a $2(r - [m - n]) + 1$ -fold degeneracy of the
 415 flat band with dispersive bands.

416 Returning to Fig. 10, note that in (a) our sets are $\{\frac{AX}{BX}, \frac{AY}{BY}\} \rightarrow \{1, 1\}$ for AB;
 417 $\{\frac{AX}{CX}, \frac{AY}{CY}\} \rightarrow \{1, 1\}$ for AC; and $\{\frac{BX}{CX}, \frac{BY}{CY}\} \rightarrow \{1, 1\}$ for BC. Since both B and C can
 418 be exchanged with A, we say that there are *two* path-exchanges. This leads to a triple
 419 degeneracy in the H_5 system. In (b) the ratios for the same pairs are $\{\alpha, \alpha\}, \{\alpha, \alpha\}$, and
 420 $\{\alpha, \alpha\}$, where $\alpha \neq 1$. Thus, we still have two path-exchanges and the degeneracy remains
 421 the same. In (c) the ratios are $\{1, 1\}, \{1, 1\}$, and $\{1, 1\}$ (despite the different hoppings) and
 422 hence the degeneracy is still 3. And finally in (d) the ratios are $\{1, 1\}, \{1, \beta\}$, and $\{1, \beta\}$.
 423 Since we reduce the number of path-exchanges in the system by 1, this lowers the degeneracy
 424 to 1 (basically lifting the degeneracy) as shown in Fig. 10(e) and (f).

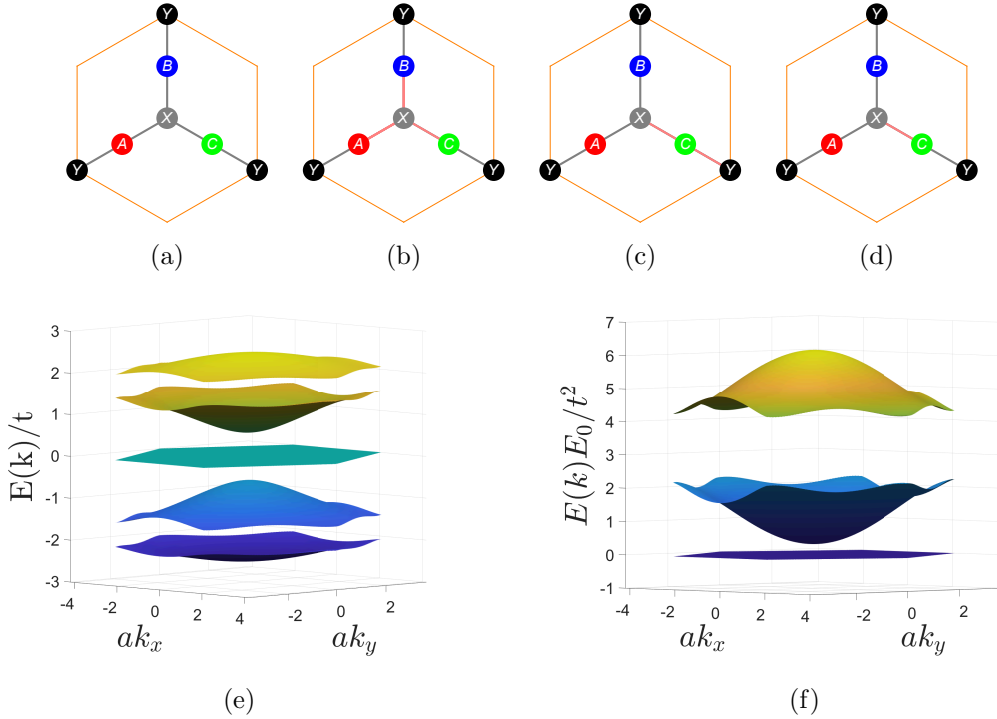


Figure 10: Hoppings in the unit cell of the H_5 system. The pink bonds are different from the grey bonds. the situations in (a), (b), and (c) do not lift the flat band degeneracy but that in (d) does. This is because, in the former three, the paths for individual atoms for going from the ABC subsystem to XY subsystem are exchangeable. Whereas in (d) that condition is broken. (e) Isolated flat band in the spectrum of the exchange-broken H_5 system and (f) the same for the projected Kagomé subsystem with the exchange-breaking perturbation being $\delta t = 0.5t$. The flat band is preserved and isolated from the dispersing bands.

425 **Note** In general, with hopping parameters $t_{G_i K_j}$, the projected Hamiltonian in the
 426 Kagomé subspace is

$$H_{\text{eff,K}} = \frac{1}{E_0} \times \begin{pmatrix} t_{G_1 K_1}^2 + t_{G_2 K_1}^2 & t_{G_1 K_1} t_{G_1 K_2} + t_{G_2 K_1} t_{G_2 K_2} e^{-i\vec{k}\cdot\vec{R}_1} & t_{G_1 K_1} t_{G_1 K_3} + t_{G_2 K_1} t_{G_2 K_3} e^{-i\vec{k}\cdot\vec{R}_2} \\ \text{c.c.} & t_{G_1 K_2}^2 + t_{G_2 K_2}^2 & t_{G_1 K_2} t_{G_1 K_3} + t_{G_2 K_2} t_{G_2 K_3} e^{-i\vec{k}\cdot(\vec{R}_2 - \vec{R}_1)} \\ \text{c.c.} & \text{c.c.} & t_{G_1 K_3}^2 + t_{G_2 K_3}^2 \end{pmatrix} \quad (18)$$

427 This form is the same as in Ref. [49] where the authors decomposed their Kagomé Hamilto-
 428 nian into contributions from ‘upper’ triangles and ‘lower triangles’. In their interpretation,
 429 in order to isolate the flat band they hypothesized breaking inversion (in the bonds) in the
 430 unit cell. This is not technically correct. It is not sufficient to break inversion at the level
 431 of the hoppings between the nearest neighbor atoms: the changes in hoppings need to
 432 be correlated in a definite manner which was only evident because of the author’s chosen
 433 parameterization. One example of inversion broken deformation of the Kagomé unit cell
 434 is the r -parameterization discussed in Sec. 2. This parameterization breaks inversion but
 435 does not lift the flat band degeneracy. To understand why, consider the H_5 Hamiltonian
 436 with the parameterization above where $t_{G_i K_j} = t$ except $t_{G_2 K_3} = t + \delta t$ and $t_{G_1 K_3} = t - \delta t$.
 437 This results in the following projected Hamiltonian in the Kagomé subspace:

$$H_{\text{eff,K}}(\Delta) = \frac{t^2}{E_0} \begin{pmatrix} 2 & 1 + e^{-i\vec{k}\cdot\vec{R}_1} & (1 - \Delta) + (1 + \Delta)e^{-i\vec{k}\cdot\vec{R}_2} \\ 1 + e^{i\vec{k}\cdot\vec{R}_1} & 2 & (1 - \Delta) + (1 + \Delta)e^{-i\vec{k}\cdot(\vec{R}_2 - \vec{R}_1)} \\ (1 + \Delta)e^{i\vec{k}\cdot\vec{R}_2} & (1 + \Delta)e^{i\vec{k}\cdot(\vec{R}_2 - \vec{R}_1)} & 2 + \Delta^2 \end{pmatrix} \quad (19)$$

438 where $\Delta = \frac{\delta t}{t}$. Notice that in the Kagomé subspace, this isn’t just an arbitrary breaking
 439 of the mirror in the Kagomé lattice as the Δ has to enter the onsite energy in precisely
 440 the stated manner to preserve the flatness of the band. However, in the H_5 system, it is
 441 sufficient to break the path-exchange symmetry in the bonds, in any manner possible with
 442 no other conditions, and we arrive at the appropriate Hamiltonian in the projected basis
 443 with all the necessary conditions built-in.

444 In this regard, we emphasize that while the statement in Ref. [49] that their stated per-
 445 turbation that isolates the flat band also breaks inversion is correct, we wish to state that
 446 breaking inversion does not necessarily gap out the flat band and that inversion may not
 447 have anything to do with the problem at hand. This is evident from the r -parameterization
 448 presented earlier which also breaks inversion but preserves the degeneracy of the flat band.

449 We note in passing that this path-exchange symmetry is a fundamental symmetry of
 450 bipartite graph. Certain spatial symmetries such as mirror, rotations, inversions can be
 451 a special case of this symmetry. It is thus easy to associate the spatial symmetries to
 452 the cause of degeneracies. This is not incorrect, but they are not fundamental. In the
 453 examples we present in this article, most of the path-exchange symmetries can be broken
 454 by breaking a mirror symmetry or a C_n symmetry in the physical lattice.

455 6 Application of the prescription to other lattices

456 Thus far we derived the well-known lattices like the Kagomé and Graphene systems as
 457 projections from a parent H_5 system and indicated that isolating the flat band requires
 458 breaking the path-exchange symmetry in their parent system. We now demonstrate that
 459 the other systems that are discussed in the literature (like Lieb and Dice) are actually
 460 the parent systems to other flat-band lattices and that the flat band could be isolated

461 by breaking the path-exchange symmetry of the parent system. We shall only show the
 462 results for the strict bipartite case to keep the discussion simple, but as we have shown,
 463 this is not needed.

464 6.1 Lieb lattice and its projections

465 The Lieb lattice shown in Fig. 11(a) is another realizable example of the prescription.
 466 The system is bipartite within the nn approximation and the Hamiltonian is given by

$$H_{\text{Lb}} = -t \begin{pmatrix} 0 & 1 + e^{-i\vec{k}\cdot\vec{R}_1} & 1 + e^{-i\vec{k}\cdot\vec{R}_2} \\ 1 + e^{i\vec{k}\cdot\vec{R}_1} & 0 & 0 \\ 1 + e^{i\vec{k}\cdot\vec{R}_2} & 0 & 0 \end{pmatrix}, \quad (20)$$

467 where all the terms have an analogous meaning as in Eq. (1), but in this case $\vec{R}_2 = (0, 1)$.
 468 Here, however, the Lieb lattice is the analog of the H_5 Hamiltonian, prior to projection.
 469 Hence, the spectrum is particle-hole symmetric as shown in Fig. 11(b).

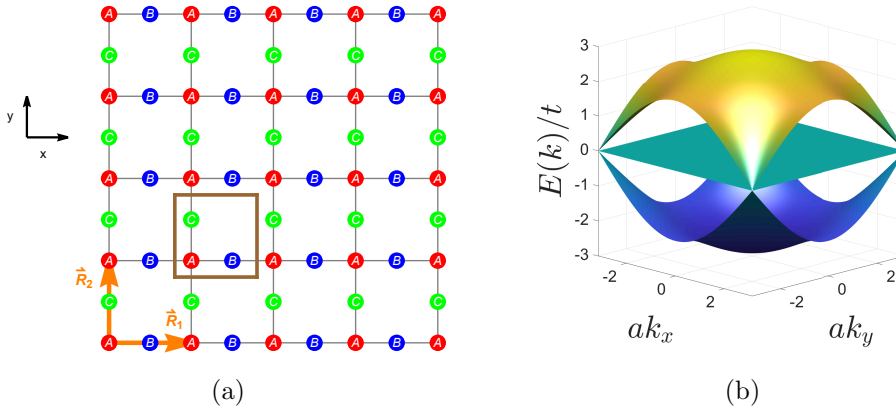


Figure 11: (a) Lieb lattice with three atoms A, B, C in the unit cell and the translation vectors \vec{R}_1 and \vec{R}_2 . (b) The energy spectrum for Lieb lattice. Note the presence of the flat band at the center of the particle-hole symmetric spectrum.

470 Carrying out the projections using the Löwdin's method, the two subsystems are

$$H_{\text{eff,Sq}}(E_0) = \frac{2t^2}{E_0} \left[2 + \cos(\vec{k} \cdot \vec{R}_1) + \cos(\vec{k} \cdot \vec{R}_2) \right], \quad (21)$$

471 which is the regular square lattice; and the other Hamiltonian is

$$H_{\text{eff,xSq}}(E_0) = \frac{t^2}{E_0} \begin{pmatrix} 2 + 2 \cos(\vec{k} \cdot \vec{R}_1) & 1 + e^{i\vec{k}\cdot\vec{R}_1} + e^{-i\vec{k}\cdot\vec{R}_2} + e^{i\vec{k}\cdot(\vec{R}_1-\vec{R}_2)} \\ 1 + e^{-i\vec{k}\cdot\vec{R}_1} + e^{i\vec{k}\cdot\vec{R}_2} + e^{-i\vec{k}\cdot(\vec{R}_1-\vec{R}_2)} & 2 + 2 \cos(\vec{k} \cdot \vec{R}_2) \end{pmatrix}, \quad (22)$$

472 which is also a square lattice with 2-atoms per unit cell, which we may refer to as the
 473 extended square lattice. The lattices and spectrum of these two effective systems are
 474 shown in Fig. 12. It is worth noting that without the projection technique, one would
 475 need to know the exact ratios of the nn and nnn hoppings to ensure the presence of the
 476 flat band in the two band system. However, this technique ensures that the projected
 477 systems already have the selected ratios to have the flat band.

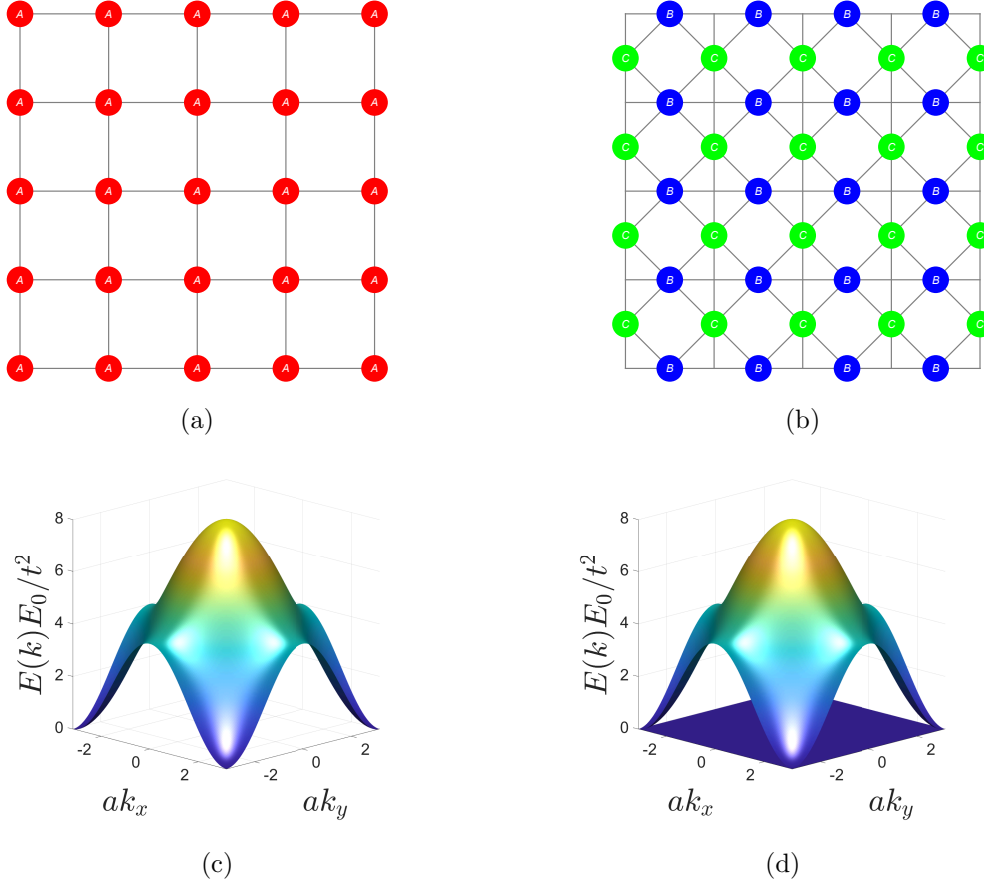


Figure 12: (a) and (b) The two subsystems (square and extended square lattices) from projecting out the Lieb lattice. (c) and (d) The energy spectrum for the respective subsystems. Note the presence of the flat band in the extended square lattice.

478 Further, like we identified H_{GK} in H_5 , one can identify the matrix H_{SX} with

$$H_{SX} = \begin{pmatrix} 1 + e^{-i\vec{k}\cdot\vec{R}_1} & 1 + e^{-i\vec{k}\cdot\vec{R}_2} \end{pmatrix}, \quad (23)$$

479 which can be generalized to

$$H_{SX} = \begin{pmatrix} t_{AB} + \tilde{t}_{AB}e^{-i\vec{k}\cdot\vec{R}_1} & t_{AC} + \tilde{t}_{AC}e^{-i\vec{k}\cdot\vec{R}_2} \end{pmatrix}. \quad (24)$$

480 We can now break the path-exchange symmetry in the Lieb lattice [see Fig. 13(b)] by
 481 selecting the parameterization $t_{AC} = (t - \delta t)$ and $\tilde{t}_{AC} = (t + \delta t)$. We show in Fig. 13(d)
 482 the spectrum of the exchange-broken Lieb lattice projected onto the extended square
 483 lattice system which shows the isolated flat band.

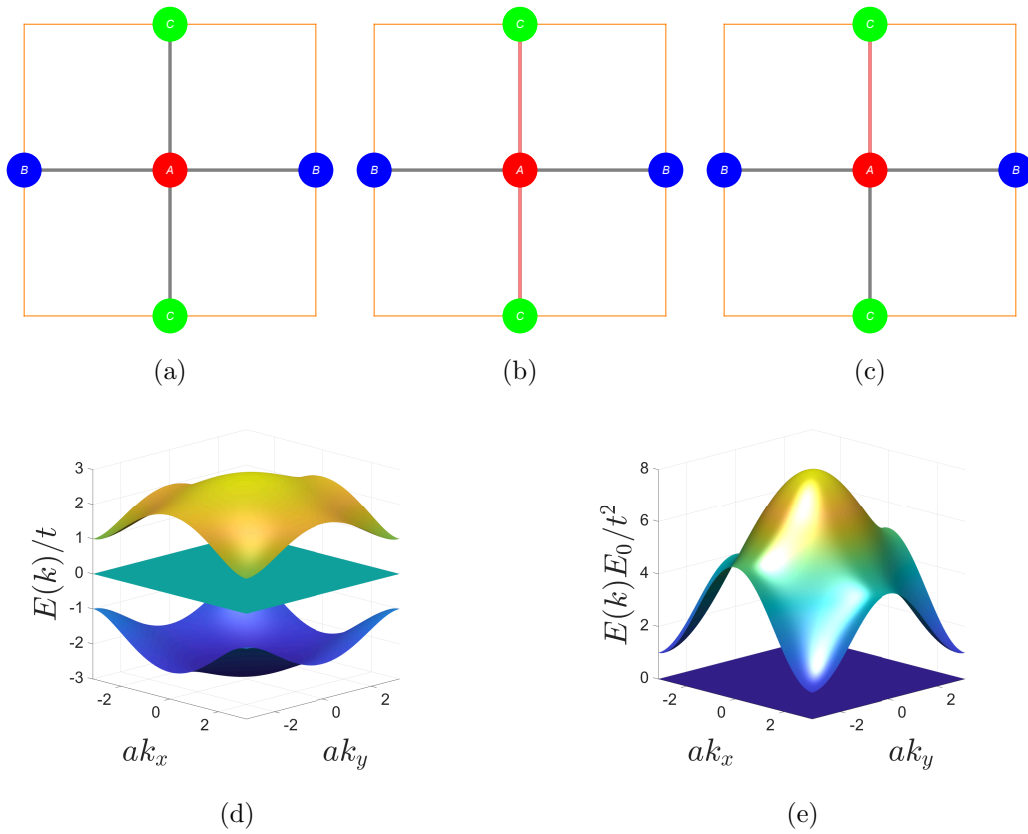


Figure 13: Hoppings in the unit cell of the Lieb lattice with A being one system and BC being the other. In situations (a) and (b), where the path-exchange between the subsystems is preserved, the flat band degeneracy is not lifted degeneracy, but it is in (c) where the condition is broken. (d) Isolated flat band in the spectrum of the exchange-broken Lieb lattice and (e) the same but projected onto the extended square lattice. Here, the exchange-breaking perturbation is $\delta t = 0.5t$.

484 **6.2 Dice lattice and its projections**

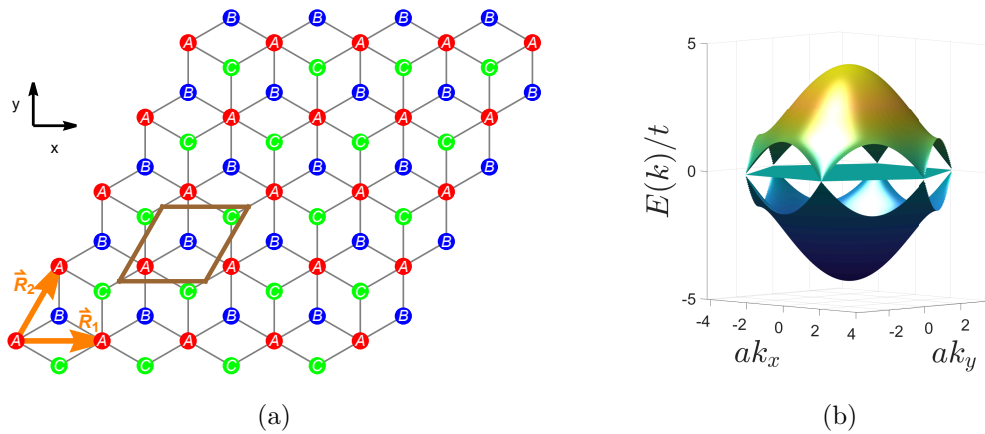


Figure 14: (a) Dice lattice with three atoms A, B, C in the unit cell and the translation vectors \vec{R}_1 and \vec{R}_2 . (b) The respective energy spectrum with the flat band as well as particle-hole symmetry.

485 The Dice lattice [shown in the Fig. 14(a)] has the following Hamiltonian:

$$H_{\text{Dc}} = -t \begin{pmatrix} 0 & 1 + e^{-i\vec{k}\cdot\vec{R}_1} + e^{-i\vec{k}\cdot\vec{R}_2} & 1 + e^{-i\vec{k}\cdot\vec{R}_1} + e^{i\vec{k}\cdot(\vec{R}_2-\vec{R}_1)} \\ 1 + e^{i\vec{k}\cdot\vec{R}_1} + e^{i\vec{k}\cdot\vec{R}_2} & 0 & 0 \\ 1 + e^{i\vec{k}\cdot\vec{R}_1} + e^{-i\vec{k}\cdot(\vec{R}_2-\vec{R}_1)} & 0 & 0 \end{pmatrix} \quad (25)$$

486 where $\vec{R}_1 = (1, 0)$ and $\vec{R}_2 = \left(\frac{1}{2}, \frac{\sqrt{3}}{2}\right)$. The two subsystems are the triangular lattice

$$H_{\text{eff,T}}(E_0) = \frac{4t^2}{E_0} \left[\frac{3}{2} + \cos(\vec{k}\cdot\vec{R}_1) + \cos(\vec{k}\cdot\vec{R}_2) + \cos(\vec{k}\cdot(\vec{R}_1 - \vec{R}_2)) \right] \quad (26)$$

487 and something which is a Graphene lattice with nnn and nnnn hoppings (which we may
488 call the extended Graphene lattice):

$$H_{\text{eff,xG}}(E_0) = \frac{t^2}{E_0} \begin{pmatrix} |h(\vec{k})|^2 & e^{-i\vec{k}\cdot\vec{R}_1} h^2(\vec{k}) \\ e^{i\vec{k}\cdot\vec{R}_1} h^{*2}(\vec{k}) & |h(\vec{k})|^2 \end{pmatrix}, \quad (27)$$

489 where $h(\vec{k}) = 1 + e^{i\vec{k}\cdot\vec{R}_1} + e^{i\vec{k}\cdot\vec{R}_2}$.

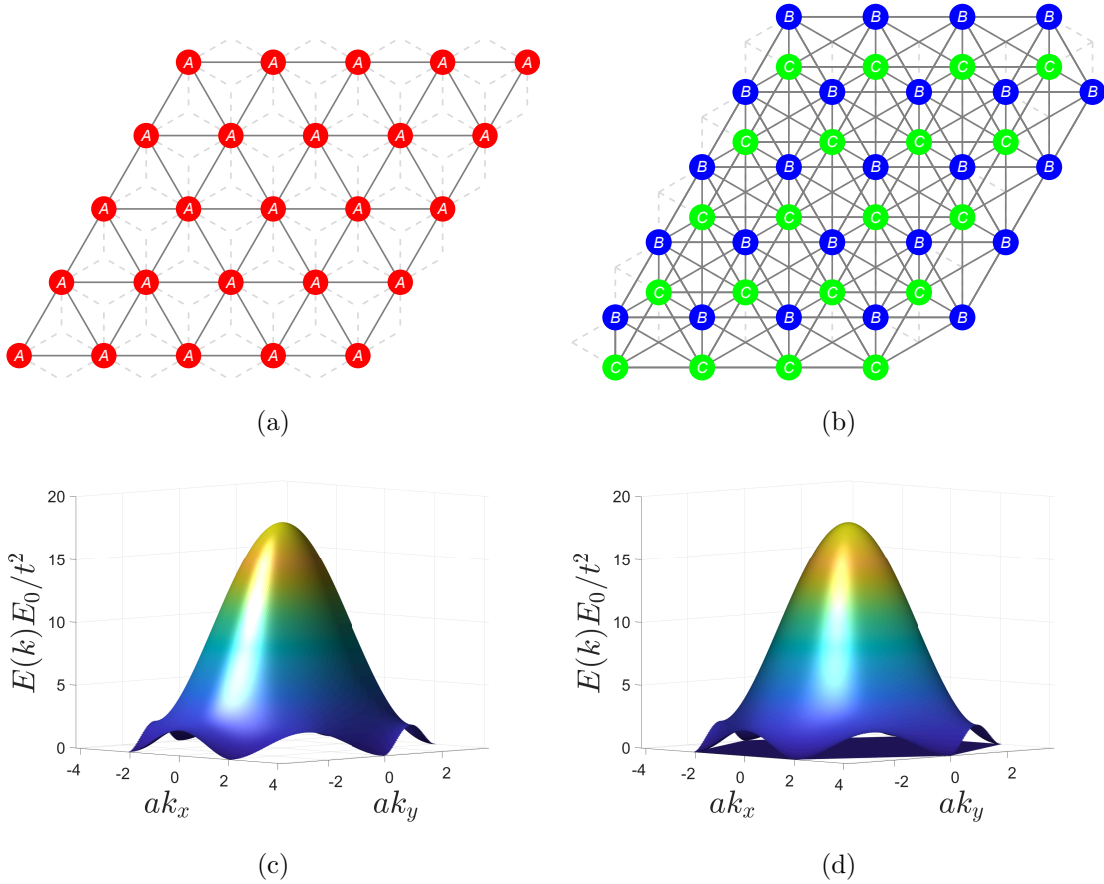


Figure 15: (a) and (b) The two projected subsystems of the Dice lattice. (c) and (d) Their respective energy dispersion. Note the flat band in the extended Graphene.

490 We can now define the following matrix

$$H_{TX} = \begin{pmatrix} t_{AB}^1 + t_{AB}^2 e^{-i\vec{k}\cdot\vec{R}_1} + t_{AB}^3 e^{-i\vec{k}\cdot\vec{R}_2} & t_{AC}^1 + t_{AC}^2 e^{-i\vec{k}\cdot\vec{R}_1} + t_{AC}^3 e^{i\vec{k}\cdot(\vec{R}_2-\vec{R}_1)} \end{pmatrix}. \quad (28)$$

491 We can now break the path-exchange symmetry in the Dice lattice [see Fig. 16(b)] by
 492 selecting the parameterization $t_{AC}^1 = (t - \delta t)$, $t_{AC}^2 = (t - \delta t)$ and $t_{AC}^3 = (t + \delta t)$. We
 493 show in Fig. 16(d) the spectrum of the exchange-broken Dice lattice projected onto the
 494 extended Graphene lattice which shows the isolated flat band.

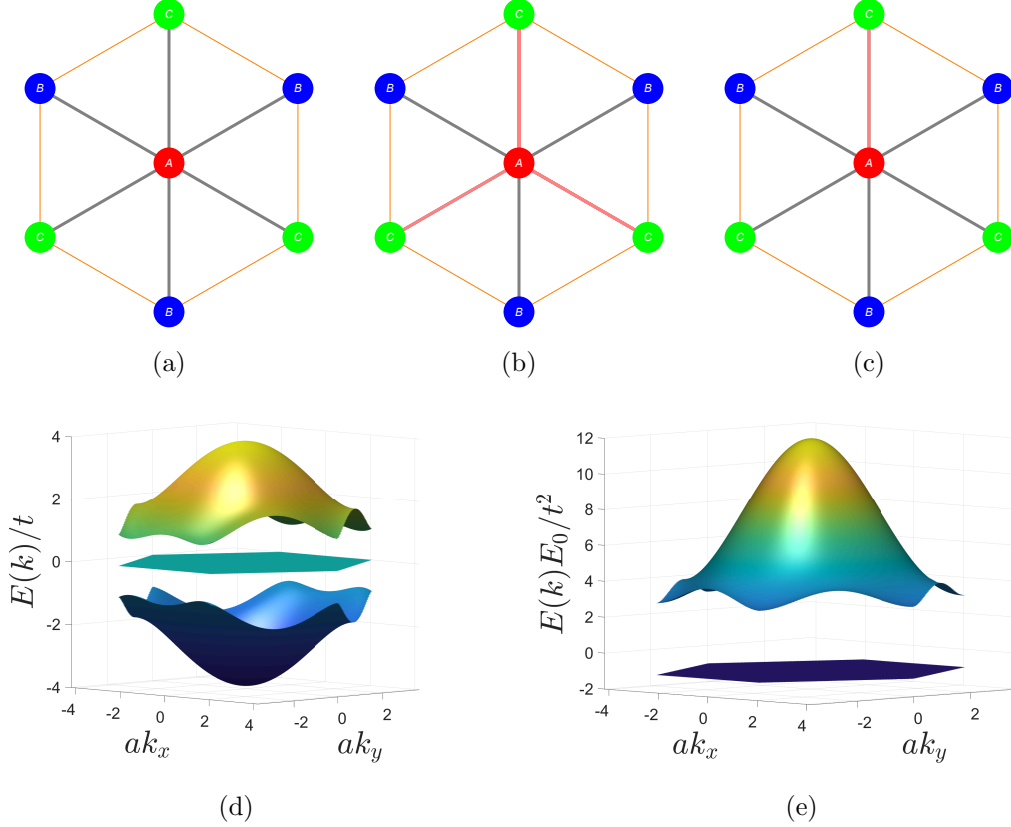


Figure 16: Hoppings in the unit cell of the Dice lattice. A is one subsystem and BC is the other. In the situations (a) and (b) the exchange-symmetry is preserved and so is the flat band degeneracy, whereas in (c) it is broken and the flat band degeneracy is lifted. (d) Isolated flat band in the spectrum of the exchange-broken Dice lattice and (e) the same but projected onto the extended Graphene lattice. Here, the exchange-breaking perturbation is $\delta t = t$.

495 7 Flat band with Chern-Simons flux distribution

496 In this section we demonstrate that the properties we outlined above also apply to systems
 497 with reduced translation symmetry such as in situations where the lattice is subject to a
 498 flux $\phi = 2\pi p/q$ per unit cell. Such a system is usually modelled as a Hofstadter problem
 499 by attaching phases on the bonds such that when the pattern is extended to the entire
 500 lattice one finds a unit cell that is enlarged q -fold.

501 First, let us note a feature of the projection of the subsystems. Although we introduced
 502 the projection in the \mathbf{k} -space, the same principles apply in the real space. This can be seen
 503 by performing a unitary transformation from the Bloch basis to tight-binding basis. It is
 504 advantageous to work in the real space as one would not have to worry about the unit-cell
 505 enlargement due to the flux attachment to the bonds. For definiteness, consider again the
 506 bipartite H_5 lattice with atoms $\{X_i, Y_i\}$ from one subsystem and $\{A_i, B_i, C_i\}$ in another

507 subsystem, where i marks the unit cell. By a direct calculation it can be shown that if
 508 one were to project out the XY subsystem then the effective hopping that is induced in
 509 the ABC subsystem, say t_{PQ} (where $P, Q \in \{A, B, C\}$), would be given by the sum of
 510 products of hoppings taking $P \rightarrow \{X, Y\} \rightarrow Q$. In the H_5 case every sum only consists
 511 of one term such that $t_{PQ} = t_{PX}t_{XQ}$ or $t_{PY}t_{YQ}$. This means that the phase associated
 512 with the effective bond PQ would be the sum of phases along the path from P to Q in
 513 the original system.

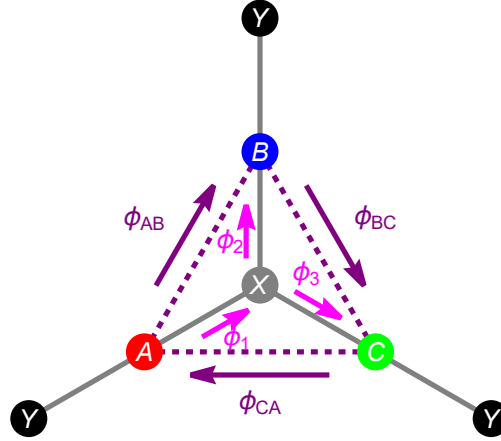


Figure 17: The hoppings inside the unit cell of the H_5 lattice, but with phases $\phi_{1,2,3}$ attached as shown. Upon projecting out the XY subsystem, the effective hoppings (dashed lines) acquire phases $\phi_{AB,BC,CA}$.

514 Second, it is clear that since we started out with a bipartite system, we would end
 515 up with a projected system with a flat band. However, it is interesting to observe the
 516 situation depicted in Fig. 17 where the parent system has phases ϕ_1 , ϕ_2 and ϕ_3 attached
 517 to the hoppings between the subsystems. Upon projection, using the result presented
 518 above, we find that $\phi_{AB} = \phi_1 + \phi_2$, $\phi_{BC} = \phi_3 - \phi_2$, and $\phi_{CA} = -\phi_3 - \phi_1$. This results
 519 in $\phi_{AB} + \phi_{BC} + \phi_{CA} = \oint \vec{A} \cdot d\vec{l} = 0$, i.e. the flux enclosed in the triangular regions is
 520 zero. This is in fact the scenario that is predicted to happen for in a Kagomé chiral spin-
 521 liquid which is modelled as fermions subject to a Chern-Simons (CS) field. Thus, the flux
 522 distribution that is implemented by the projection technique naturally accounts for the
 523 CS nature of the flux distribution and is probably a good tool to use to model systems
 524 with CS fields. It follows from this that in a Maxwell-like flux distribution (where the flux
 525 is proportional to the area enclosed, see Fig. 18), a flat band is not guaranteed. This is the
 526 reason why lattices with Maxwell-like fluxes have dispersive bands (in general), whereas
 527 those with CS-type fluxes can have flat bands. This comparison has been discussed in Fig.
 528 4 of Ref. [27]. In that work, it was also pointed out that the flat band was gapped from
 529 the other dispersive bands. This is now easy to understand (e.g., see Fig. 19) that the
 530 path-exchange symmetry is broken due to the phase attachments, which isolates the flat
 531 band.

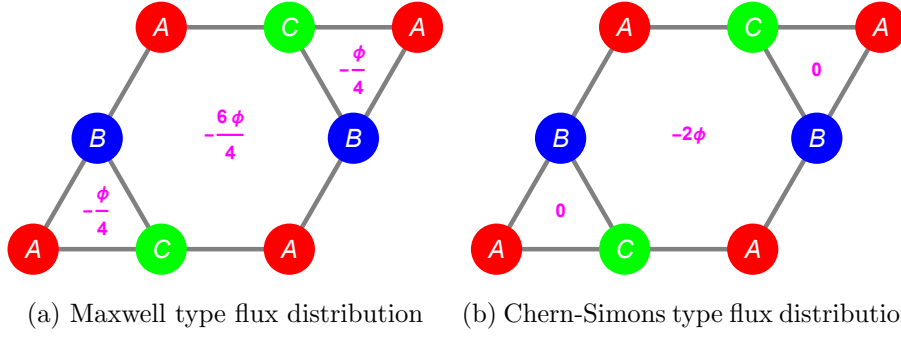


Figure 18: Under Maxwell type field, the flux is proportional to area whereas in the CS case, the flux is concentrated in one region of the unit cell, with the triangular parts having zero flux.

532 As an explicit example let us consider the case with $\phi = \pi$. Here the unit cell is
 533 doubled ($q = 2$). The Hamiltonian is given by

$$H^{\phi=\pi} = \begin{pmatrix} 0 & H_{GK}^{\pi} \\ H_{KG}^{\pi} & 0 \end{pmatrix}, \quad (29)$$

534 where

$$H_{KG}^{\pi} = -t \begin{pmatrix} 1 & 0 & 0 & e^{-i\vec{k}\cdot\vec{R}_2} \\ 0 & e^{-i\pi} & e^{-i\vec{k}\cdot\vec{R}_2} & 0 \\ 1 & 0 & 1 & 0 \\ 0 & 1 & 0 & 1 \\ 1 & 0 & e^{i\vec{k}\cdot(\vec{R}_1-\vec{R}_2)} & 0 \\ 0 & e^{-i\pi} & 0 & e^{i\vec{k}\cdot(\vec{R}_1-\vec{R}_2)} \end{pmatrix} \quad (30)$$

535 and $R_1 = (1, 0)$ and $R_2 = (\frac{1}{2}, \frac{\sqrt{3}}{2})$. The phase attachments are shown in Fig. 19 and the
 536 band structure for the H_5 system and the projected systems are shown in Fig. 20, which
 537 clearly show the isolated flat band. This feature remains for all values of $\phi \in (0, 2\pi)$.

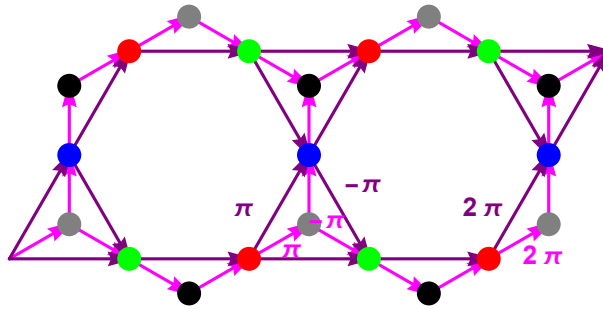


Figure 19: Chern-Simons flux attachment prescription for $\phi = \pi$. All the flux is concentrated on the middle hexagon and the flux through the triangular regions is zero. The unit cell is doubled. The purple lines indicate the hoppings in the projected subsystem and each parallelogram formed by these lines is the original unit cell. The pink lines represent the hoppings of the parent system. The arrows indicate the phases, which are all zero except the three in purple and pink each with $(\pi, -\pi, 2\pi)$.

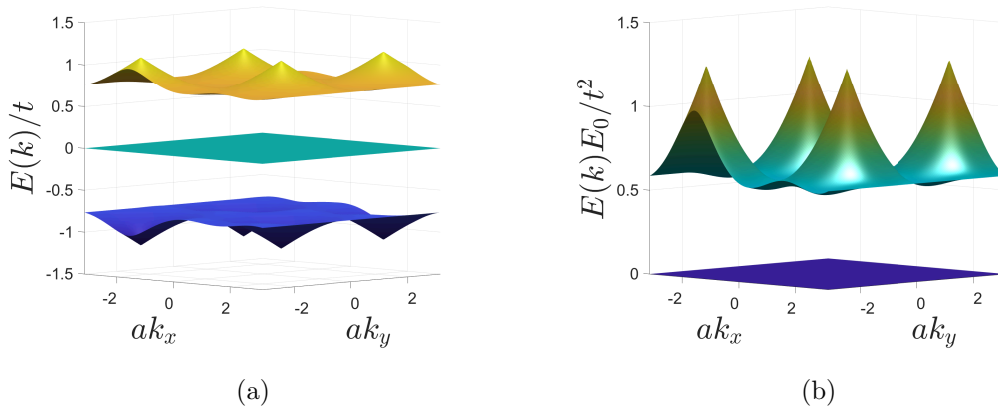


Figure 20: (a) Energy spectrum of H_5 with CS field with flux $\phi = \pi$ (b) Energy spectrum of $H_{\text{eff,K}}$. In both cases notice the flat band at $E = 0$. We are only showing the bands closest to the flat band.

538 8 Conclusion

539 Although there exist many works in the literature on designing systems with flat bands,
 540 they suffer from one or many of the following shortcomings: the need for long-ranged
 541 hoppings; the need for fine-tuning of parameters even with nn approximation; the need for
 542 staggered fluxes. While these are all valid techniques, they could be seen as shortcomings
 543 because implementing long-range hoppings is often a design challenge. So is fine-tuning
 544 parameters of the Hamiltonian. Breaking a discrete symmetry such as the time-reversal
 545 symmetry is certainly viable, however, generating staggered flux may not always be a
 546 straightforward task. In this work, we proposed a straightforward design method based
 547 on the bipartiteness of a system (which is not strictly necessary) and Löwdin's projection to
 548 generate flat band systems. In this prescription, we were able to identify that if there exists
 549 a path-exchange symmetry in the bipartite system, with different sizes of the subsystems,
 550 the flat band would appear degenerate with other dispersive bands. And by breaking
 551 the symmetry, it is possible to isolate the flat band. We then showed that projecting
 552 out various subsystems from this parent bipartite system still leaves behind a subsystem
 553 with an isolated flat band. We demonstrated the verity of all the above points of the
 554 prescription by applying it to the H_5 lattice (from which we can project out the hexagonal
 555 lattice and the Kagomé lattice: the latter having the spectrum of the former plus a flat
 556 band), Lieb and Dice lattices (from which we can project out the square and triangular
 557 lattices, respectively, and special lattices that share their respective spectra plus a flat
 558 band). We also showed that relaxing the bipartite condition in the subsystem that is
 559 being projected out still maintains the flat band. In this sense, we only need to couple a
 560 non-hopping (or weakly hopping) system to a background system, which is smaller in size,
 561 to get a flat band.

562 Apart from this main result, we even developed a special parameterization of the
 563 Kagomé lattice to show that it is possible to devise flat band conditions, different from what
 564 is already in the literature and showed that this construction is automatically implemented
 565 if arrived at from the parent bipartite system. We even showed that starting from the
 566 parent bipartite system, we can reproduce the conditions for the existence and isolation of
 567 flat bands that were discussed previously in the literature (about staggered π fluxes [42]
 568 and inversion broken Kagomé [49]). Finally, we demonstrated that the existence of a flat

569 band in the chiral spin-liquid state of the Kagomé lattice that originates due to coupling
 570 to a Chern Simons like field is also consistent with the rules we identify in this work. This
 571 also suggests that the Chern Simons type flux in lattices could be understood in terms of
 572 Maxwellian flux coupled to bipartite systems.

573 We also believe that the prescription suggested here should be practically imple-
 574 mentable in photonic-crystal lattices or even in cavity QED techniques such as in Refs.
 575 [54, 55]. Isolating the various subsystems can be done, e.g. simply by introducing appro-
 576 priate onsite energies to split the subsystems in energy, and then tuning the energy scale
 577 of any probe to be near the respective onsite energies of interest. This will a subject for
 578 a future work.

579 There are several interesting avenues to pursue using this construction. It may be
 580 possible to study the role of electronic correlations in Kagomé and Graphene by studying
 581 them in the parent H_5 system. Given that we have a systematic way to isolate flat
 582 bands, it can serve as a test bench to investigate fractional Quantum Hall state formation
 583 in the absence of a magnetic field. Further, it was stated in Ref. [41] that the band
 584 touching was protected by topology in the Kagomé system. However, we have seen that
 585 the band touching is protected by a path exchange symmetry in a parent bipartite system.
 586 This could suggest a connection between topology and exchange-symmetries in a higher-
 587 dimensional Hilbert space. It will also be interesting to explore the link between the
 588 path-exchange symmetry and the Shubnikov groups as elaborated on in Ref. [52].

589 Acknowledgments

590 The authors would like to acknowledge useful exchanges with A. Andreanov.

591 **Funding information** This work was funded by the Natural Sciences and Engineering
 592 Research Council of Canada (NSERC) Grant No. RGPIN-2019-05486 (S.M.).

593 APPENDIX

594 A Useful relations between matrix elements $\tilde{\alpha}_i$

There are a couple of identities involving the matrix elements of the Hamiltonian that can be derived straightforwardly. For the parameter $|r| < 1$, we observe that

$$|\tilde{\alpha}_i|^2 = 2e^{-h}[\cosh h + \cos(\vec{k} \cdot \vec{R}_i)],$$

and the quantity $A = 2\text{Re}[\tilde{\alpha}_1^* \tilde{\alpha}_2 \tilde{\alpha}_3^*]$ evaluates to

$$A = 2[1 + (e^{-h} + e^{-2h}) \sum_i \cos(\vec{k} \cdot \vec{R}_i) + e^{-3h}].$$

Using these we arrive at the relation

$$\sum_i |\tilde{\alpha}_i|^2 = 2e^{-h}[3 \cosh h + \sum_i \cos(\vec{k} \cdot \vec{R}_i)].$$

595 Observing that both $\sum_i |\tilde{\alpha}_i|^2$ and A have $\sum_i \cos(\vec{k} \cdot \vec{R}_i)$ in them as the only \vec{k} -dependent
 596 term, it is possible to search for f that satisfies the flat band condition in Eq. (5) by
 597 equating their coefficients, which leads to $f = 2e^{-\frac{h}{2}} \cosh \frac{h}{2}$.

598 If $|r| > 1$, then the identification $\frac{1-r}{1+r} = e^{-h}$ can still be made if h is extended to
 599 the complex plane. In particular, we note that as $|r| > 1$, h acquires a step jump in
 600 the imaginary part from 0 to $\pm i\pi$. The sign is ambiguous but this does not affect our
 601 analysis and we shall stick to the choice of $i\pi$. That is, $h \rightarrow h_c$ such that $e^{-\text{Re}[h]} = \frac{r-1}{r+1}$.
 602 This extension to the complex plane also results in $[e^{-h_c}]^* = e^{-h_c}$, thus acting like a real
 603 number. This ensures that all the above identities above are still valid with $h \rightarrow h_c$. In
 604 that case, the resulting parameter f is given by $f = 2e^{-\frac{h_c}{2}} \cosh \frac{h_c}{2} = 2e^{-\frac{\text{Re}h_c}{2}} \sinh \frac{\text{Re}h_c}{2}$,
 605 where $\frac{1-r}{1+r} = e^{-\text{Re}h_c}$.

606 B Properties of non-square matrices

Consider a non-square matrix $M_{n \times m}$ with $m > n$ for definiteness. Two square matrices
 could be constructed from this: $[MM^\dagger]_{n \times n}$ and $[M^\dagger M]_{m \times m}$. Now construct the square
 matrix $\tilde{M}_{m \times m}$ by padding $m - n$ rows of zero to M . Then we have

$$\tilde{M}\tilde{M}^\dagger = \begin{pmatrix} [MM^\dagger]_{n \times n} & 0_{n \times (n-m)} \\ 0_{n \times (n-m)} & 0_{(n-m) \times (n-m)} \end{pmatrix}$$

and

$$\tilde{M}^\dagger \tilde{M} = M^\dagger M.$$

607 From properties of matrices we have $\text{Det}[\tilde{M}\tilde{M}^\dagger] = \text{Det}[\tilde{M}^\dagger \tilde{M}]$ which is the product of their
 608 eigenvalues. Since $\tilde{M}\tilde{M}^\dagger$ explicitly has $m - n$ 0's as eigenvalues, and that this construction
 609 is possible for any M , it follows that $\tilde{M}^\dagger \tilde{M}$ and hence $M^\dagger M$ must have (i) the same number
 610 of 0 eigenvalues; (ii) the same non-zero eigenvalues.

611 In other words, what we have argued is that for a non-square matrix $M_{n \times m}$, MM^\dagger
 612 and $M^\dagger M$ have the same eigenvalues with one of them having $|n - m|$ zeros as additional
 613 eigenvalues.

614 C Identifying the path-exchange symmetry

615 Consider a generic flat band system generated based on a bipartite system whose subsys-
 616 tems have size $n \times n$ and $m \times m$ with $n < m$. In such a system, there are $m - n$ flat
 617 bands at $E = 0$. This means that there are $m - n$ additional redundant equations (rows)
 618 in the system for any \mathbf{k} . If the flat bands are additionally degenerate with any of the other
 619 dispersive bands at a particular \mathbf{k} -point, then at that \mathbf{k} -point there must be additional
 620 equations (rows) that are redundant. A redundant equation (row) can be reduced to a
 621 scaled version of the other linearly independent equations (rows). For generic scenarios
 622 in nn bipartite systems, it is sufficient to just look at the scaling property. In a bipartite
 623 system of the form

$$\hat{H} = \begin{pmatrix} 0 & \hat{h}_{n \times m}^\dagger \\ \hat{h}_{m \times n} & 0 \end{pmatrix} \quad (81)$$

624 all the information is contained in the block $\hat{h}_{m \times n}$, which has m equations and n unknowns.
 625 If such a system has $E = 0$ solutions, then only n of these are linearly independent. If
 626 one identifies r rows that could be scaled (we call them r zero rows), then linear algebra
 627 dictates that there would be $p = 2(r - [m - n]) + 1$ degeneracies in the system. That is,
 628 for every new row, we introduce two degeneracies. The factor of 2 arises from the fact
 629 that each time we reduce a row in \hat{h} , we reduce one in \hat{h}^\dagger (this won't be the case for

630 non-bipartite cases as will be discussed shortly). To extract the physical meaning behind
 631 this, note that each redundant row, if not trivially zero, is a scaled version of the linearly
 632 independent rows. Since a given row in the \hat{h} block contains the hopping from one atom,
 633 say A , of larger subsystem to all the other atoms of the smaller subsystem, the redundancy
 634 of another row would imply that another atom, say B , from the larger subsystem has a
 635 scaled set of hoppings of A . That is, the set $\{AX_i\}$ and set $\{BX_i\}$ (where $\{X_i\}$ is the
 636 set of atoms in the smaller subsystem) are related via $\{AX_i\} = \alpha\{BX_i\}$. If AX_i and
 637 BX_i are not trivial, then we can construct the set of ratios $\{\frac{AX_i}{BX_i}\}$. A redundancy of a
 638 row requires the set $\{\frac{AX_i}{BX_i}\}$ to be a unit set and we say that the paths from A and from
 639 B are exchangeable. In simpler terms, for a bipartite system, for r path-exchanges we
 640 would have $2(r - [m - n]) + 1$ degeneracies. Thus, breaking/reducing the number of path-
 641 exchanges would lift/reduce the degeneracies. In this sense r simply counts the number
 642 of atoms in the larger subsystem that could be exchanged. If we now consider the system

$$\hat{H} = \begin{pmatrix} \hat{s}_{n \times n} & \hat{h}_{n \times m}^\dagger \\ \hat{h}_{m \times n} & 0 \end{pmatrix}, \quad (32)$$

643 where \hat{s} is non-trivial, then for r path-exchanges, we would have $p = (r - [m - n]) + 1$
 644 degeneracies. We lose the factor of 2 due to presence of \hat{s} .

645 As an example, consider the bipartite H_5 lattice with $m = 3, n = 2$. Here the formula
 646 that applies is $p = 2(r - 1) + 1 = 2r - 1$. The number of reducible rows (r) can be 1 or 2.
 647 Thus, we can have a degeneracy p of 1 (non degenerate) or 3 (triply degenerate) at $E = 0$
 648 or none. So, if the \hat{h} block looks like

$$\begin{pmatrix} t_1 & t_2 \\ t_3 & t_4 e^{i\vec{k} \cdot \vec{R}_1} \\ t_5 & t_6 e^{i\vec{k} \cdot \vec{R}_2} \end{pmatrix}, \quad (33)$$

649 the case with two path-exchanges would look like

$$\frac{t_3}{t_1} = \frac{t_4 e^{i\vec{k} \cdot \vec{R}_1}}{t_2}, \quad \text{and} \quad \frac{t_6 e^{i\vec{k} \cdot \vec{R}_2}}{t_2} = \frac{t_5}{t_1}, \quad (34)$$

650 then $p = 2(2 - [m - n]) + 1 = 3$, a triple degeneracy. Because the hoppings are real,
 651 this condition is only satisfied at the Γ -point ($\mathbf{k} = 0$). Breaking any of the path-exchange
 652 reduces the degeneracy by 2 and hence removing the degeneracy in this case.

653 References

- 654 [1] L. Balents, C. R. Dean, D. K. Efetov and A. F. Young, *Superconductivity*
 655 *and strong correlations in moiré flat bands*, Nature Physics **16**(7), 725 (2020),
 656 doi:10.1038/s41567-020-0906-9.
- 657 [2] E. Y. Andrei, D. K. Efetov, P. Jarillo-Herrero, A. H. MacDonald, K. F. Mak,
 658 T. Senthil, E. Tutuc, A. Yazdani and A. F. Young, *The marvels of moiré mate-*
 659 *rials*, Nature Reviews Materials **6**(3), 201 (2021), doi:10.1038/s41578-021-00284-1.
- 660 [3] Y. Cao, V. Fatemi, S. Fang, K. Watanabe, T. Taniguchi, E. Kaxiras and P. Jarillo-
 661 Herrero, *Unconventional superconductivity in magic-angle graphene superlattices*, Na-
 662 ture **556**(7699), 43 (2018), doi:10.1038/nature26160.

- 663 [4] Y. Cao, V. Fatemi, A. Demir, S. Fang, S. L. Tomarken, J. Y. Luo, J. D. Sanchez-
664 Yamagishi, K. Watanabe, T. Taniguchi, E. Kaxiras, R. C. Ashoori and P. Jarillo-
665 Herrero, *Correlated insulator behaviour at half-filling in magic-angle graphene super-*
666 *lattices*, Nature **556**(7699), 80 (2018), doi:10.1038/nature26154.
- 667 [5] P. M. Eugenio and C. B. Dağ, *DMRG study of strongly interacting \mathbb{Z}_2 flatbands: a*
668 *toy model inspired by twisted bilayer graphene*, SciPost Phys. Core **3**, 015 (2020),
669 doi:10.21468/SciPostPhysCore.3.2.015.
- 670 [6] A. Yazdani, *Magic, symmetry, and twisted matter*, Science **371**(6534), 1098
671 (2021), doi:10.1126/science.abg5641, [https://www.science.org/doi/pdf/10.](https://www.science.org/doi/pdf/10.1126/science.abg5641)
672 [1126/science.abg5641](https://www.science.org/doi/pdf/10.1126/science.abg5641).
- 673 [7] M. Oh, K. P. Nuckolls, D. Wong, R. L. Lee, X. Liu, K. Watanabe, T. Taniguchi
674 and A. Yazdani, *Evidence for unconventional superconductivity in twisted bilayer*
675 *graphene*, Nature **600**(7888), 240 (2021), doi:10.1038/s41586-021-04121-x.
- 676 [8] X. Liu, C.-L. Chiu, J. Y. Lee, G. Farahi, K. Watanabe, T. Taniguchi, A. Vishwanath
677 and A. Yazdani, *Spectroscopy of a tunable moiré system with a correlated and topo-*
678 *logical flat band*, Nature Communications **12**(1), 2732 (2021), doi:10.1038/s41467-
679 021-23031-0.
- 680 [9] A. Lau, S. Peotta, D. I. Pikulin, E. Rossi and T. Hyart, *Universal suppression*
681 *of superfluid weight by non-magnetic disorder in s-wave superconductors indepen-*
682 *dent of quantum geometry and band dispersion*, SciPost Phys. **13**, 086 (2022),
683 doi:10.21468/SciPostPhys.13.4.086.
- 684 [10] I. Syôzi, *Statistics of Kagomé Lattice*, Progress of Theoretical Physics **6**(3), 306
685 (1951), doi:10.1143/ptp/6.3.306, [https://academic.oup.com/ptp/article-pdf/](https://academic.oup.com/ptp/article-pdf/6/3/306/5239621/6-3-306.pdf)
686 [6/3/306/5239621/6-3-306.pdf](https://academic.oup.com/ptp/article-pdf/6/3/306/5239621/6-3-306.pdf).
- 687 [11] E. H. Lieb, *Two theorems on the hubbard model*, Phys. Rev. Lett. **62**, 1201 (1989),
688 doi:10.1103/PhysRevLett.62.1201.
- 689 [12] B. Sutherland, *Localization of electronic wave functions due to local topology*, Phys.
690 Rev. B **34**, 5208 (1986), doi:10.1103/PhysRevB.34.5208.
- 691 [13] T. Kida, L. A. Fenner, A. A. Dee, I. Terasaki, M. Hagiwara and A. S. Wills, *The*
692 *giant anomalous hall effect in the ferromagnet fe3sn2—a frustrated kagome metaa*
693 *frustrated kagome metal*, Journal of Physics: Condensed Matter **23**(11), 112205
694 (2011), doi:10.1088/0953-8984/23/11/112205.
- 695 [14] J. Ruostekoski, *Optical kagome lattice for ultracold atoms with nearest neighbor inter-*
696 *actions*, Phys. Rev. Lett. **103**, 080406 (2009), doi:10.1103/PhysRevLett.103.080406.
- 697 [15] G.-B. Jo, J. Guzman, C. K. Thomas, P. Hosur, A. Vishwanath and D. M. Stamper-
698 Kurn, *Ultracold atoms in a tunable optical kagome lattice*, Phys. Rev. Lett. **108**,
699 045305 (2012), doi:10.1103/PhysRevLett.108.045305.
- 700 [16] G.-W. Chern and A. Saxena, *Pt-symmetric phase in kagome-based photonic lattices*,
701 Opt. Lett. **40**(24), 5806 (2015), doi:10.1364/OL.40.005806.
- 702 [17] Z. Li, J. Zhuang, L. Wang, H. Feng, Q. Gao, X. Xu, W. Hao, X. Wang, C. Zhang,
703 K. Wu, S. X. Dou, L. Chen *et al.*, *Realization of flat band with possible non-*
704 *trivial topology in electronic kagome lattice*, Science Advances **4**(11), eaau4511

- 705 (2018), doi:10.1126/sciadv.aau4511, <https://www.science.org/doi/pdf/10.1126/sciadv.aau4511>.
- 706
- 707 [18] B. Cui, X. Zheng, J. Wang, D. Liu, S. Xie and B. Huang, *Realization of lieb lat-*
708 *tice in covalent-organic frameworks with tunable topology and magnetism*, Nature
709 Communications **11**(1), 66 (2020), doi:10.1038/s41467-019-13794-y.
- 710 [19] D. Leykam, A. Andreanov and S. Flach, *Artificial flat band systems: from*
711 *lattice models to experiments*, Advances in Physics: X **3**(1), 1473052 (2018),
712 doi:10.1080/23746149.2018.1473052, [https://doi.org/10.1080/23746149.2018.](https://doi.org/10.1080/23746149.2018.1473052)
713 1473052.
- 714 [20] M. Lacki, J. Zakrzewski and N. Goldman, *A dark state of Chern bands: De-*
715 *signing flat bands with higher Chern number*, SciPost Phys. **10**, 112 (2021),
716 doi:10.21468/SciPostPhys.10.5.112.
- 717 [21] D. Varjas, A. Abouelkomsan, K. Yang and E. J. Bergholtz, *Topological lat-*
718 *tice models with constant Berry curvature*, SciPost Phys. **12**, 118 (2022),
719 doi:10.21468/SciPostPhys.12.4.118.
- 720 [22] E. Tang, J.-W. Mei and X.-G. Wen, *High-temperature fractional quantum hall states*,
721 Phys. Rev. Lett. **106**, 236802 (2011), doi:10.1103/PhysRevLett.106.236802.
- 722 [23] D. T. Son, *Is the composite fermion a Dirac particle?*, Phys. Rev. X **5**, 031027 (2015),
723 doi:10.1103/PhysRevX.5.031027.
- 724 [24] S. Maiti and T. A. Sedrakyan, *Composite fermion state of graphene*
725 *as a Haldane-Chern insulator*, Phys. Rev. B **100**, 125428 (2019),
726 doi:10.1103/PhysRevB.100.125428.
- 727 [25] T. A. Sedrakyan and A. V. Chubukov, *Fermionic propagators for two-*
728 *dimensional systems with singular interactions*, Phys. Rev. B **79**, 115129 (2009),
729 doi:10.1103/PhysRevB.79.115129.
- 730 [26] T. A. Sedrakyan, L. I. Glazman and A. Kamenev, *Spontaneous formation of a nonuni-*
731 *form chiral spin liquid in a moat-band lattice*, Phys. Rev. Lett. **114**, 037203 (2015),
732 doi:10.1103/PhysRevLett.114.037203.
- 733 [27] S. Maiti and T. Sedrakyan, *Fermionization of bosons in a flat band*, Phys. Rev. B
734 **99**, 174418 (2019), doi:10.1103/PhysRevB.99.174418.
- 735 [28] G. V. Dunne, *Aspects of Chern-Simons theory*, arXiv (1998).
- 736 [29] R. Wang, Z. Y. Xie, B. Wang and T. Sedrakyan, *Emergent topological orders and*
737 *phase transitions in lattice Chern-Simons theory of quantum magnets*, Phys. Rev. B
738 **106**, L121117 (2022), doi:10.1103/PhysRevB.106.L121117.
- 739 [30] R. Wang, B. Wang and T. Sedrakyan, *Chern-Simons superconductors and their*
740 *instabilities*, Phys. Rev. B **105**, 054404 (2022), doi:10.1103/PhysRevB.105.054404.
- 741 [31] E. Dagotto, E. Fradkin and A. Moreo, *A comment on the nielsen-ninomiya the-*
742 *orem*, Physics Letters B **172**(3), 383 (1986), doi:[https://doi.org/10.1016/0370-](https://doi.org/10.1016/0370-2693(86)90274-1)
743 2693(86)90274-1.
- 744 [32] S. Sachdev and J. Ye, *Gapless spin-fluid ground state in a random quantum Heisenberg*
745 *magnet*, Phys. Rev. Lett. **70**, 3339 (1993), doi:10.1103/PhysRevLett.70.3339.

- 746 [33] A. Kitaev, *A simple model of quantum holography (part 1)*, Proceedings of the KITP
747 Program: Entanglement in Strongly-Correlated Quantum Matter (2015).
- 748 [34] A. Kitaev, *A simple model of quantum holography (part 2)*, Proceedings of the KITP
749 Program: Entanglement in Strongly-Correlated Quantum Matter (2015).
- 750 [35] L. García-Álvarez, I. L. Egusquiza, L. Lamata, A. del Campo, J. Sonner and
751 E. Solano, *Digital quantum simulation of minimal AdS/CFT*, Phys. Rev. Lett.
752 **119**, 040501 (2017), doi:10.1103/PhysRevLett.119.040501.
- 753 [36] I. Danshita, M. Hanada and M. Tezuka, *Creating and probing the Sachdev–Ye–Kitaev
754 model with ultracold gases: Towards experimental studies of quantum grav-
755 ity*, Progress of Theoretical and Experimental Physics **2017**(8) (2017),
756 doi:10.1093/ptep/ptx108, 083I01, [https://academic.oup.com/ptep/article-pdf/
757 2017/8/083I01/19650704/ptx108.pdf](https://academic.oup.com/ptep/article-pdf/2017/8/083I01/19650704/ptx108.pdf).
- 758 [37] D. I. Pikulin and M. Franz, *Black hole on a chip: Proposal for a physical realization of
759 the Sachdev–Ye–Kitaev model in a solid-state system*, Phys. Rev. X **7**, 031006 (2017),
760 doi:10.1103/PhysRevX.7.031006.
- 761 [38] A. Chen, R. Ilan, F. de Juan, D. I. Pikulin and M. Franz, *Quantum holography in
762 a graphene flake with an irregular boundary*, Phys. Rev. Lett. **121**, 036403 (2018),
763 doi:10.1103/PhysRevLett.121.036403.
- 764 [39] C. Wei and T. A. Sedrakyan, *Optical lattice platform for the Sachdev–Ye–Kitaev
765 model*, Phys. Rev. A **103**, 013323 (2021), doi:10.1103/PhysRevA.103.013323.
- 766 [40] C. Wei and T. A. Sedrakyan, *Quantum chaos, superconductivity, and informa-
767 tion scrambling in disordered magic-angle twisted bilayer graphene*, arXiv:2205.09766
768 (2022).
- 769 [41] D. L. Bergman, C. Wu and L. Balents, *Band touching from real-space
770 topology in frustrated hopping models*, Phys. Rev. B **78**, 125104 (2008),
771 doi:10.1103/PhysRevB.78.125104.
- 772 [42] D. Green, L. Santos and C. Chamon, *Isolated flat bands and spin-1 con-
773 ical bands in two-dimensional lattices*, Phys. Rev. B **82**, 075104 (2010),
774 doi:10.1103/PhysRevB.82.075104.
- 775 [43] W. Maimaiti, A. Andreanov, H. C. Park, O. Gendelman and S. Flach, *Compact
776 localized states and flat-band generators in one dimension*, Phys. Rev. B **95**, 115135
777 (2017), doi:10.1103/PhysRevB.95.115135.
- 778 [44] W. Maimaiti, S. Flach and A. Andreanov, *Universal $d = 1$ flat band
779 generator from compact localized states*, Phys. Rev. B **99**, 125129 (2019),
780 doi:10.1103/PhysRevB.99.125129.
- 781 [45] W. Maimaiti, A. Andreanov and S. Flach, *Flat-band generator in two dimensions*,
782 Phys. Rev. B **103**, 165116 (2021), doi:10.1103/PhysRevB.103.165116.
- 783 [46] M. Röntgen, C. V. Morfonios and P. Schmelcher, *Compact localized states and
784 flat bands from local symmetry partitioning*, Phys. Rev. B **97**, 035161 (2018),
785 doi:10.1103/PhysRevB.97.035161.
- 786 [47] C. V. Morfonios, M. Röntgen, M. Pyzh and P. Schmelcher, *Flat bands by latent
787 symmetry*, Phys. Rev. B **104**, 035105 (2021), doi:10.1103/PhysRevB.104.035105.

- 788 [48] A. Mallick, N. Chang, A. Andreanov and S. Flach, *Anti- \mathcal{PT} flatbands*, Phys. Rev. A
789 **105**, L021305 (2022), doi:10.1103/PhysRevA.105.L021305.
- 790 [49] T. Bilitewski and R. Moessner, *Disordered flat bands on the kagome lattice*, Phys.
791 Rev. B **98**, 235109 (2018), doi:10.1103/PhysRevB.98.235109.
- 792 [50] Y. Xu and H. Pu, *Building flat-band lattice models from gram matrices*, Phys. Rev.
793 A **102**, 053305 (2020), doi:10.1103/PhysRevA.102.053305.
- 794 [51] S. M. Zhang and L. Jin, *Flat band in two-dimensional non-hermitian optical lattices*,
795 Phys. Rev. A **100**, 043808 (2019), doi:10.1103/PhysRevA.100.043808.
- 796 [52] D. Călugăru, A. Chew, L. Elcoro, Y. Xu, N. Regnault, Z.-D. Song and B. A. Bernevig,
797 *General construction and topological classification of crystalline flat bands*, Nature
798 Physics **18**(2), 185 (2022), doi:10.1038/s41567-021-01445-3.
- 799 [53] N. Regnault, Y. Xu, M.-R. Li, D.-S. Ma, M. Jovanovic, A. Yazdani, S. S. P. Parkin,
800 C. Felser, L. M. Schoop, N. P. Ong, R. J. Cava, L. Elcoro *et al.*, *Catalogue of flat-*
801 *band stoichiometric materials*, Nature **603**(7903), 824 (2022), doi:10.1038/s41586-
802 022-04519-1.
- 803 [54] J. Koch, A. A. Houck, K. L. Hur and S. M. Girvin, *Time-reversal-symmetry*
804 *breaking in circuit-QED-based photon lattices*, Phys. Rev. A **82**, 043811 (2010),
805 doi:10.1103/PhysRevA.82.043811.
- 806 [55] A. J. Kollár, M. Fitzpatrick, P. Sarnak and A. A. Houck, *Line-graph lattices:*
807 *Euclidean and non-euclidean flat bands, and implementations in circuit quantum*
808 *electrodynamics*, Communications in Mathematical Physics **376**(3), 1909 (2020),
809 doi:10.1007/s00220-019-03645-8.
- 810 [56] C. S. Chiu, D.-S. Ma, Z.-D. Song, B. A. Bernevig and A. A. Houck, *Fragile topology*
811 *in line-graph lattices with two, three, or four gapped flat bands*, Phys. Rev. Research
812 **2**, 043414 (2020), doi:10.1103/PhysRevResearch.2.043414.
- 813 [57] F. de Juan, J. L. Mañes and M. A. H. Vozmediano, *Gauge fields from strain in*
814 *graphene*, Phys. Rev. B **87**, 165131 (2013), doi:10.1103/PhysRevB.87.165131.
- 815 [58] A. L. Kitt, V. M. Pereira, A. K. Swan and B. B. Goldberg, *Erratum: Lattice-corrected*
816 *strain-induced vector potentials in graphene [phys. rev. b 85, 115432 (2012)]*, Phys.
817 Rev. B **87**, 159909 (2013), doi:10.1103/PhysRevB.87.159909.
- 818 [59] M. Oliva-Leyva and G. G. Naumis, *Understanding electron behavior in strained*
819 *graphene as a reciprocal space distortion*, Phys. Rev. B **88**, 085430 (2013),
820 doi:10.1103/PhysRevB.88.085430.
- 821 [60] M. Ramezani Masir, D. Moldovan and F. Peeters, *Pseudo magnetic field in*
822 *strained graphene: Revisited*, Solid State Communications **175-176**, 76 (2013),
823 doi:https://doi.org/10.1016/j.ssc.2013.04.001, Special Issue: Graphene V: Recent Ad-
824 vances in Studies of Graphene and Graphene analogues.
- 825 [61] G. Montambaux, F. Piéchon, J.-N. Fuchs and M. O. Goerbig, *Merging of*
826 *dirac points in a two-dimensional crystal*, Phys. Rev. B **80**, 153412 (2009),
827 doi:10.1103/PhysRevB.80.153412.

- 828 [62] L.-K. Lim, J.-N. Fuchs, F. Piéchon and G. Montambaux, *Dirac points emerg-*
829 *ing from flat bands in lieb-kagome lattices*, Phys. Rev. B **101**, 045131 (2020),
830 doi:10.1103/PhysRevB.101.045131.
- 831 [63] L. Du, Q. Chen, A. D. Barr, A. R. Barr and G. A. Fiete, *Floquet hofstadter*
832 *butterfly on the kagome and triangular lattices*, Phys. Rev. B **98**, 245145 (2018),
833 doi:10.1103/PhysRevB.98.245145.
- 834 [64] R. Schaffer, Y. Huh, K. Hwang and Y. B. Kim, *Quantum spin liquid in a breathing*
835 *kagome lattice*, Phys. Rev. B **95**, 054410 (2017), doi:10.1103/PhysRevB.95.054410.
- 836 [65] P. Löwdin, *A note on the quantum-mechanical perturbation theory*, The Journal of
837 Chemical Physics **19**(11), 1396 (1951), doi:10.1063/1.1748067, [https://doi.org/](https://doi.org/10.1063/1.1748067)
838 [10.1063/1.1748067](https://doi.org/10.1063/1.1748067).